

Accepted Manuscript

Investigating molecular dynamics-guided lead optimization of EGFR inhibitors

Martin J. Lavecchia, Raimon Puig de la Bellacasa, José I. Borrell, Claudio N. Cavasotto

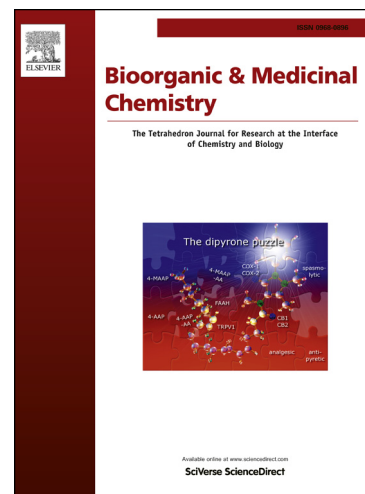
PII: S0968-0896(15)30211-X
DOI: <http://dx.doi.org/10.1016/j.bmc.2015.12.046>
Reference: BMC 12739

To appear in: *Bioorganic & Medicinal Chemistry*

Received Date: 28 October 2015
Revised Date: 18 December 2015
Accepted Date: 28 December 2015

Please cite this article as: Lavecchia, M.J., Bellacasa, R.P.d., Borrell, J.I., Cavasotto, C.N., Investigating molecular dynamics-guided lead optimization of EGFR inhibitors, *Bioorganic & Medicinal Chemistry* (2015), doi: <http://dx.doi.org/10.1016/j.bmc.2015.12.046>

This is a PDF file of an unedited manuscript that has been accepted for publication. As a service to our customers we are providing this early version of the manuscript. The manuscript will undergo copyediting, typesetting, and review of the resulting proof before it is published in its final form. Please note that during the production process errors may be discovered which could affect the content, and all legal disclaimers that apply to the journal pertain.



Investigating molecular dynamics-guided lead optimization of EGFR inhibitors

Martin J. Lavecchia^{1,#}, Raimon Puig de la Bellacasa^{2,#}, José I. Borrell², Claudio N. Cavasotto^{1,*}

¹ Instituto de Investigación en Biomedicina de Buenos Aires (IBioBA) - CONICET - Partner Institute of the Max Planck Society, Godoy Cruz 2390, C1425FQD, Buenos Aires, Argentina.

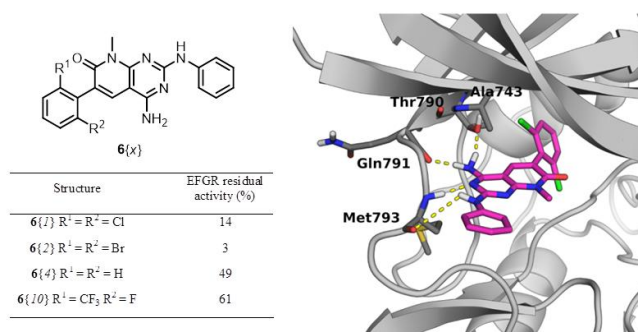
² Grup d'Enginyeria Molecular (GEM), IQS School of Engineering, Universitat Ramon Llull, Via Augusta 390 Barcelona E-08017, Spain.

* Corresponding author: Claudio N. Cavasotto, Tel: +54 11 4899-5500 e-mail cnc@cavasotto-lab.net, ccavasotto@ibioba-mpsp-conicet.gov.ar

Equally contributed to this work.

E-mail addresses: lavecchia@gmail.com [mailto:\(M.J. Lavecchia\); raimon.puig@iqs.url.edu](mailto:mailto:(M.J. Lavecchia); raimon.puig@iqs.url.edu) (R. Puig de la Bellacasa); j.i.borrell@iqs.url.edu (J.I. Borrell); cnc@cavasotto-lab.net, ccavasotto@ibioba-mpsp-conicet.gov.ar (C.N. Cavasotto).

Graphical abstract



Keywords

EGFR; molecular docking; molecular dynamics; ligand binding free energy calculation; MM/GBSA; small-molecule inhibitor; pyrido[2,3-*d*]pyrimidine; hit-to-lead optimization.

Abbreviations

EGFR, Epidermal Growth Factor Receptor; MD, molecular dynamics; MM/GBSA, Molecular Mechanics/Generalized Born Surface Area; MM/PBSA, Molecular Mechanics/Poisson-Boltzmann Surface Area; TK, Tyrosine Kinase; Generalized Amber Force Field (GAFF); Solvent-accessible Surface Area (SASA); TKI, Tyrosine Kinase Inhibitor; PDB, Protein Data Bank.

Abstract

The Epidermal Growth Factor Receptor (EGFR) is part of an extended family of proteins that together control aspects of cell growth and development, and thus a validated target for drug discovery. We explore in this work the suitability of a molecular dynamics-based end-point binding free energy protocol to estimate the relative affinities of a virtual combinatorial library designed around the EGFR model inhibitor **6{1}** as a tool to guide chemical synthesis toward the most promising compounds. To investigate the validity of this approach, selected analogues including some with better and worse predicted affinities relative to **6{1}** were synthesized, and their biological activity determined. To understand the binding determinants of the different analogues, hydrogen bonding and van der Waals contributions, and water molecule bridging in the EGFR-analogue complexes were analyzed. The experimental validation was in good qualitative agreement with our theoretical calculations, while also a 6-dibromophenyl-substituted compound with enhanced inhibitory effect on EGFR compared to the reference ligand was obtained.

1. Introduction

The epidermal growth factor receptor (EGFR) is one of the members of the family of tyrosine kinases (TKs) that are involved in the modulation of growth factor signaling. Receptors in this family contain an extracellular ligand binding domain, a transmembrane region, and an intracellular tyrosine kinase domain. Upon binding to a growth factor, receptors in this family dimerize, thus activating their kinase domain, and triggering intracellular signaling pathways, which control tumor cell growth, proliferation, survival, metastasis and angiogenesis¹.

Mutations that lead to EGFR overexpression (known as upregulation) have been associated with a number of cancers, including mammary^{2, 3}, ovarian⁴, esophageal⁵, squamous cell head and neck carcinomas⁶, non-small cell lung cancer⁷, glioblastoma⁸, where it correlates with poor prognosis⁹. Consequently, a huge effort has been poured in the development of anticancer drugs directed targeting EGFR¹⁰ which include, on one side, monoclonal antibodies targeting the extracellular domain, such as cetuximab (Erbix) for colon cancer¹¹, and, on the other hand, EGFR-specific tyrosine kinase inhibitors (TKIs) targeting the receptor catalytic domain, such as gefitinib (**1**, Iressa)¹² and erlotinib (**2**, Tarceva)¹³ for lung cancer (Figure 1)¹⁴, and dual inhibitors, such as lapatinib (EGFR/ErbB2)¹⁵ and vandetanib (EGFR/VEGFR, vascular endothelial growth factor receptor); others are under clinical trials. However, somatic mutations in the kinase domain of EGFR induce drug resistance^{14, 16, 17}. For example, erlotinib and gefitinib, which are effective in treating non-small cell lung cancer tumors harboring a mutated form of EGFR, are ineffective against EGFR variants found in glioblastoma^{8, 18, 19}. This, coupled with the fact that small modifications to TKIs could have a strong influence in the binding mode and kinetics²⁰, has encouraged sustained efforts to develop small-molecule ATP-competitive EGFR inhibitors which target both wild type and mutated forms.

In this context, functionalized pyrido[2,3-*d*]pyrimidin-7(8*H*)-ones comprise a privileged scaffold for pharmacologically active compounds with well-known activity as TKIs. More particularly, 4-unsubstituted compounds of general structure **3** have shown IC₅₀ in the range μM to nM in front of PDGFR, FGFR, EGFR, and c-Src particularly when R¹ and R⁴ are aryl groups (Figure 1)²¹⁻²³.

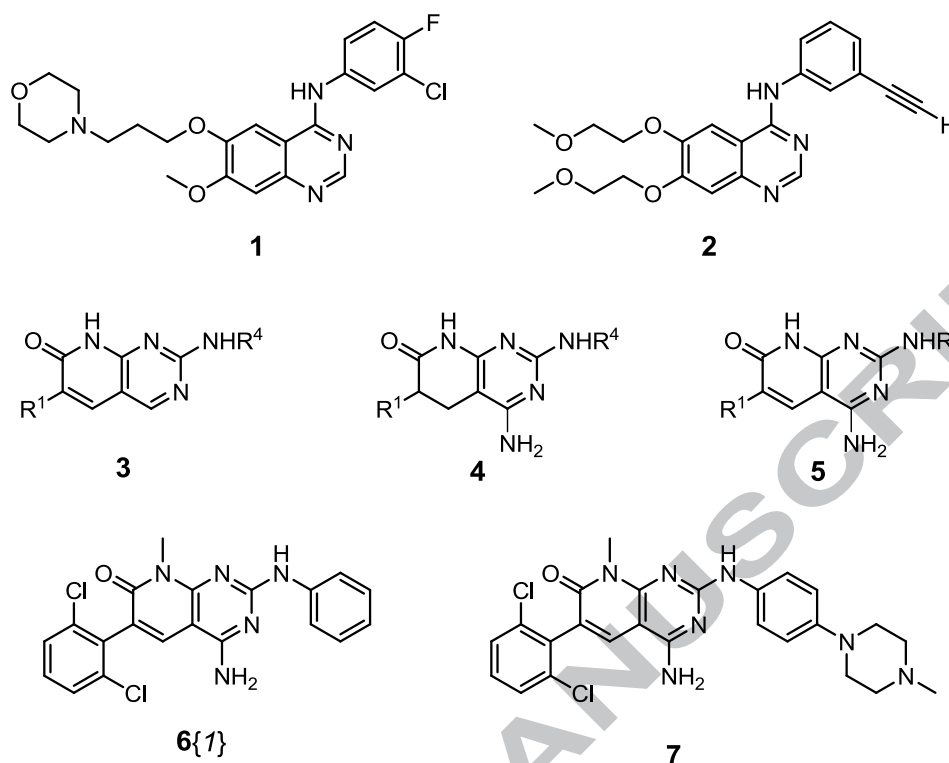


Figure 1. Structures of gefitinib (1), erlotinib (2), 4-unsubstituted pyrido[2,3-*d*]pyrimidin-7(8*H*)-ones (3), 4-amino-5,6-dihydropyrido[2,3-*d*]pyrimidin-7(8*H*)-ones (4), 4-aminopyrido[2,3-*d*]pyrimidin-7(8*H*)-ones (5), and 2,6-dichlorophenyl substituted pyridopyrimidines 6{1} and 7.

As part of our ongoing research in the area of TKIs we have described microwave assisted synthetic methodologies to access 2-aryl amino substituted 4-amino-5,6-dihydropyrido[2,3-*d*]pyrimidin-7(8*H*)-ones (4, R¹ and R⁴ = aryl) (Ref.²⁴ and references therein) and the corresponding dehydrogenated compounds 5 (Figure 1)²⁵. Using such methodologies we have recently described the synthesis of compound 7 active against non-Hodgkin's lymphomas (NHLs) by inhibiting the most upstream tyrosine kinases in the B cell receptor (BCR) signaling pathway which are involved in the mature B cell neoplasms (Figure 1)²⁶. The precursor 6{1} (Figure 1) of compound 7 also presented inhibitory activities against relevant TKs including EGFR. Interestingly, 4-amino substituted pyridopyrimidines 6{1} and 7 presented very low cellular toxicity on normal cells, contrary to 4-unsubstituted compounds 3, thus showing the importance of the 4-amino substituent. Of note, compounds 6{1} and 7 bear at position C6 the 2,6-dichlorophenyl substituent that has been widely used in the field of TKIs due to its favored fitting into the hydrophobic back pocket adjacent to the ATP binding site present in different TKs.

Today, computational methods play a critical role in lead discovery and optimization²⁷⁻³¹. In this work, we investigate the suitability of a molecular dynamics (MD)-based end-point binding free energy protocol to estimate the relative affinities of a series of congeneric compounds for EGFR as a tool to guide chemical synthesis toward the most (*in silico*) promising compounds. The MM/GBSA method used in this work has been successfully evaluated to re-score docking poses³² (cf. also the applicability of the related MM/PBSA method³³). While end-point methods based on classical mechanics are known to fail to correctly estimate binding free energies in certain cases³⁴, MM/GBSA approaches were successfully used to estimate relative binding free energies in several molecular systems³⁵⁻³⁷.

Starting with our EGFR model inhibitor 6{1}, its binding mode was assessed using

flexible molecular docking in dihedral coordinates and MD, in order to properly account for protein flexibility³⁸; from there, a virtual combinatorial library around **6{I}** was designed. In order to investigate the validity of our methodology, selected analogues including some with better and worse calculated binding affinities relative to **6{I}** were synthesized, and their biological activity determined. Analysis of the EGFR-analogue interaction in terms of hydrogen bonding, van der Waals contribution, and water molecule bridging was undertaken in order to understand the binding determinants of the different analogues. The experimental validation was in good qualitative agreement with our theoretical calculations, while we also obtained a 6-dibromophenyl-substituted molecule with improved performance toward EGFR compared to the reference ligand.

2. Results and discussion

2.1. Characterization of the binding pose of ligand **6{I}** and its interaction with EGFR.

The optimized structure of ligand **6{I}** was docked into the ligand binding site of EGFR using a two-stage protocol of rigid receptor docking followed by a full flexible docking approach, similar to what has been done on other receptors³⁹⁻⁴¹ (see Methods). The collected poses were classified as “favorable” and “unfavorable”, according to their interaction pattern (see Figure 2). It can be seen that the unfavorable pose has no hydrogen bonds with the receptor, while the favorable pose of ligand **6{I}** exhibits the following hydrogen bonds: O(Gln791)⋯HN(C4), Oγ1(Thr790)⋯HN(C4), N3⋯HN(Met793), and O(Met793)⋯HN. These residues are situated in the “hinge” region of the kinase, which connects the N and C lobes. Moreover, one of the chlorine atoms in the favorable pose makes a van der Waals contact with the amide group of Ala743.

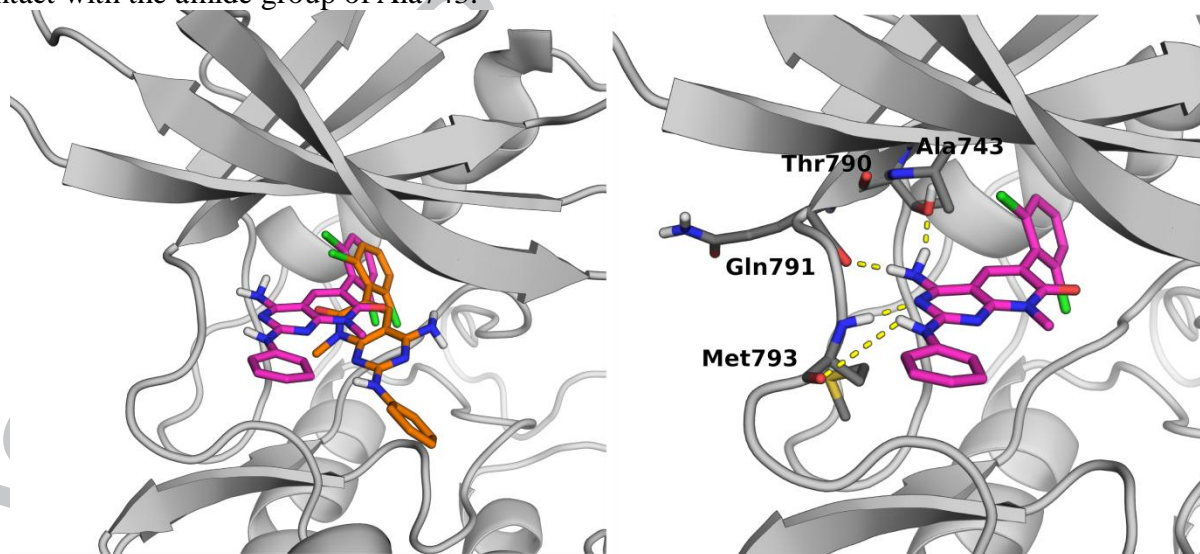


Figure 2. Favorable (magenta) and unfavorable (orange) poses of the ligand **6{I}** within the binding site (left panel). Interactions with the receptor for the favorable pose of ligand **6{I}** are shown on the right panel.

To further validate these results, and obtain a more detailed picture of the ligand-EGFR interaction, molecular dynamics (MD) simulations were carried out on both poses, and the relative binding energy estimated. An equilibration phase was performed, consisting of 1000 steps of minimization with the complex fixed, followed by 50 ps of NVT (0 to 300 K) simulation for heating the system and water equilibration. Then, 150 ps of NPT (1 atm, 300 K) simulation was carried out to relax the box size. Finally, a production phase of 40 ns in a

NPT ensemble (1 atm, 300 K) was run. Figure 3 shows the RMSD for heavy atoms of **6{I}** in the “favorable” and “unfavorable” poses throughout the production phase (cf. Figure S1 for the RMSD of the EGFR backbone atoms throughout the simulation). The calculated binding energy using the MM/GBSA method of the “unfavorable” pose relative to the favorable one was +20.5(0.1) kcal mol⁻¹, in full agreement with the qualitative analysis from the docking results, and henceforth, only the “favorable” pose will be considered as starting point for the simulations.

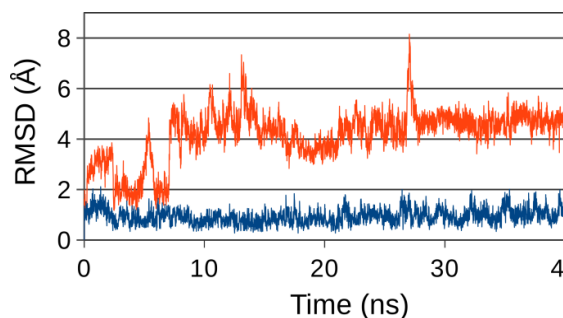


Figure 3. RMSD of “favorable” (blue) and “unfavorable” (red) poses of ligand **6{I}**, in complex with EGFR through 40 ns of the production phase (NPT ensemble, 1 atm, 300 K).

In order to compare the interaction of this ligand with other EGFR inhibitors, the EGFR-**6{I}** complex was superimposed with some of the available experimental EGFR structures complexed with other known ligands. Figure 4 shows the superposition of **6{I}** to gefitinib (PDB: 2ITY)⁴² and erlotinib (PDB: 1M17)⁴³ bound to EGFR. The main fragments of these ligands, as well as the aromatic rings with substituents, are placed in a similar location as in ligand **6{I}**, though it should be mentioned that those ligands they interact directly with the “hinge” region by only one hydrogen bond with Met793. Comparison of **6{I}** and the pyrazolo[3,4-*d*]pyrimidin-5-amine derivative described in Ref.⁴⁴ also shows a similar binding pattern.

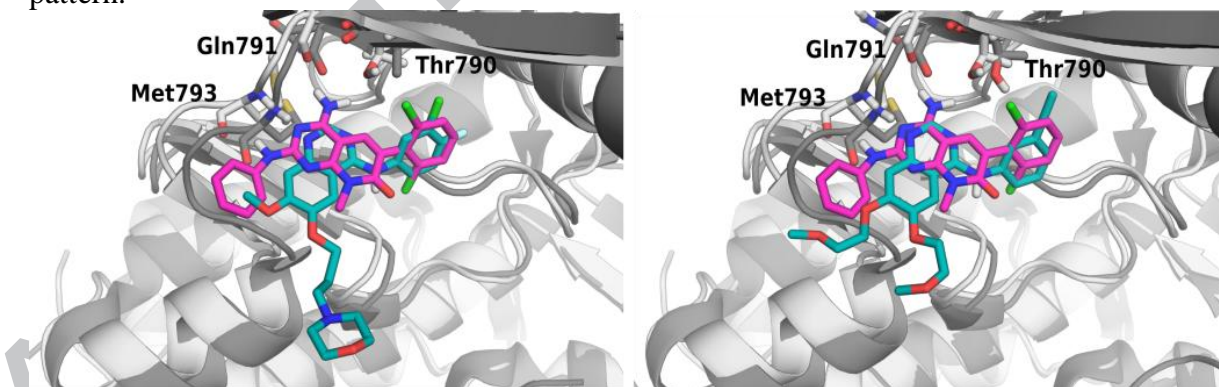


Figure 4. Binding pose of ligand **6{I}** (magenta color, receptor carbon atoms are in light grey color) overlapped with erlotinib (PDB: 1M17, left) and gefitinib (PDB: 2ITY, right). Residues Thr790, Gln791, and Met793 are shown in stick representation.

Figure 5 shows the hydrogen bond time evolution of ligand **6{I}** with the hinge region throughout the simulation. The hydrogen bonds N3...HN(Met793), and O(Met793)...HN exhibit a conserved interaction throughout the simulation. In the case of O(Gln791)...HN(C4), and Oγ1(Thr790)...HN(C4) two main conformations are visited, since the rotation around amino group, bounded to C4, is not restricted.

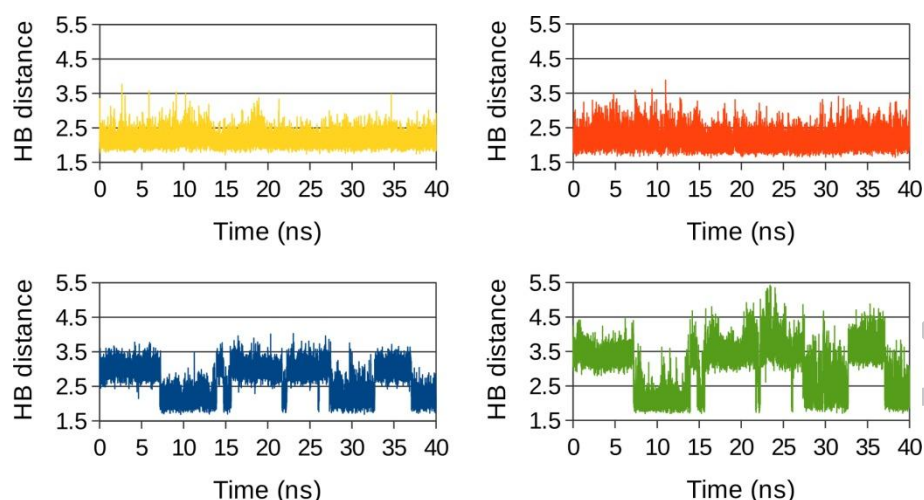


Figure 5. Time dependence of hydrogen bond (HB) distances between H atom and acceptor atom of hydrogen bonds present in favorable pose of ligand **6{1}** : N3...HN(Met793) (yellow), O(Met793)...HN (red), O(Gln791)...HN(C4) (blue), O γ 1(Thr790)...HN(C4) (green). In those bonds where the NH₂ group is involved, distance was measured only for one of the two H atoms.

2.2. *In Silico* design and characterization of ligand **6{1}** analogues

With the aim to design ligands with enhanced activity toward EGFR, a chemical library of small-molecule analogues was generated from ligand **6{x}** (Table 1). These molecules were generated by substitution of the chlorine atoms with synthetic feasible groups. Taking into consideration that ring A is constrained to rotate within the binding site (Figure 6), in those molecules where substituents R¹ and R² were different, both combinations were generated (labeled **6{Na}** and **6{Nb}**, respectively), assuming that R¹ refers to the substituent pointing toward the binding site.

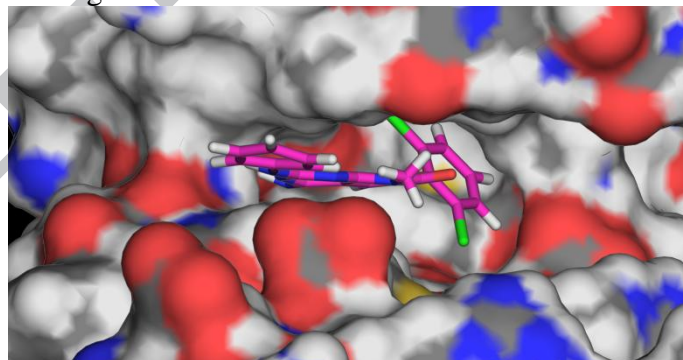


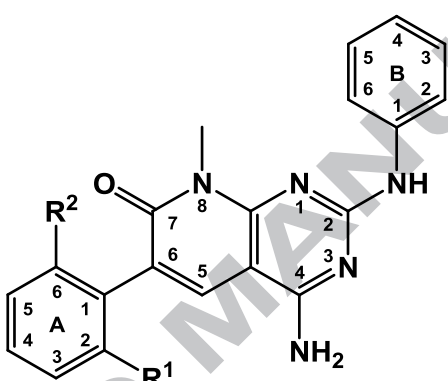
Figure 6. Ligand **6{1}** within the binding side of EGFR showing the hindered rotation of aromatic ring A.

The complex between EGFR-**6{1}** obtained from the last frame of MD trajectory was considered as the starting point to build protein-ligand complexes with molecules **6{2-11b}**. Then, 1000 steps of minimization were applied, followed by 20 ns of NPT (1 atm, 300K) simulation. This protocol was also applied to ligand **6{1}**. To estimate binding free energies, we expected the MM/GBSA to be suitable for this case^{45, 46}, though other methods could be also valid⁴⁷. On Table 1 the binding energies calculated using the MM/GBSA method are listed ($\Delta G'$), where given the structural similarity throughout the series, the ligand and receptor entropic contributions upon binding were assumed constant, and thus have not been included [cf. Eq. (1), Experimental Section]; it should be stressed that the entropic

contribution of the solvent is *de facto* accounted for in the solvation term. Following an analysis of the MM/GBSA energy (electrostatic energy, electrostatic and nonpolar contribution to the solvation energy, and van der Waals contribution), it could be seen that the van der Waals energy term (ΔE_{vdW} , see Table 1) had the highest correlation with the binding energy, a hint that the differential interaction with the receptor could be governed by that contribution.

Based on these results, two compounds with better and worse predicted affinity than **6{1}** were selected to advance to synthesis: **6{2}**, with $R^1 = R^2 = \text{Br}$, and **6{10}**, with $R^1 = \text{F}$ and $R^2 = \text{CF}_3$. As a reference, **6{4}**, with $R^1 = R^2 = \text{H}$ was also included, to shed light on the impact of substituents on ring A.

Table 1. Binding energies ($\Delta G'$, kcal mol⁻¹) and van der Waals contribution (ΔE_{vdW} , kcal mol⁻¹) calculated using MM/GBSA. The values in parentheses represent the standard error of the mean.

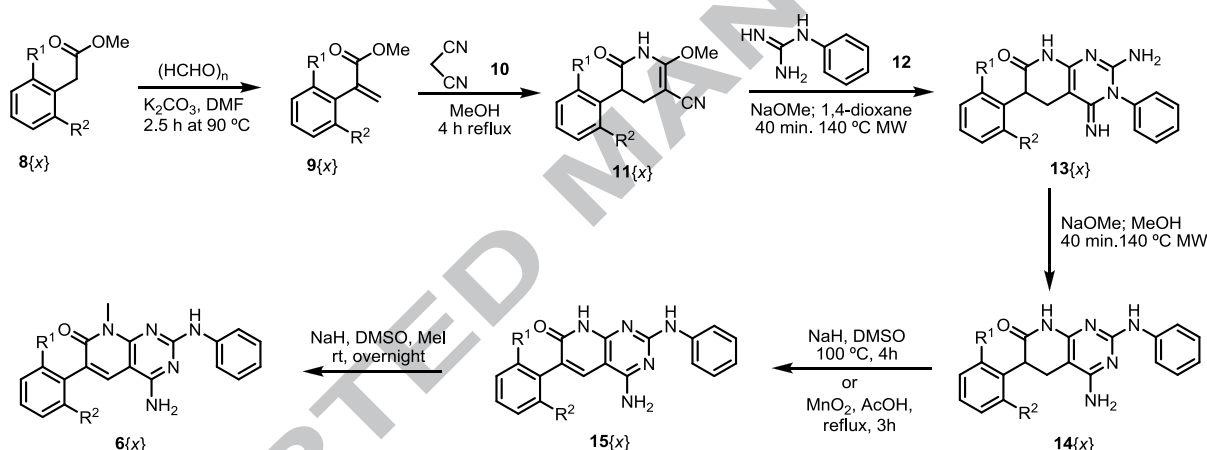


The chemical structure shows a central pyrazole ring (ring B) with an amino group (NH₂) at position 4 and an NH group at position 1. It is connected at position 2 to a pyridine ring (ring A). The pyridine ring has substituents R¹ at position 2 and R² at position 6. The pyrazole ring is also connected at position 5 to a carbonyl group (C=O) which is part of a five-membered ring containing a nitrogen atom (N) at position 8. The pyridine ring atoms are numbered 1 to 6, and the pyrazole ring atoms are numbered 1 to 5. The carbonyl carbon is numbered 7, and the nitrogen in the five-membered ring is numbered 8.

Compound	R ¹	R ²	MM-GBSA	
			ΔE_{vdW}	$\Delta G'$
6{1}	Cl	Cl	-51.2 (0.1)	-49.5 (0.1)
6{2}	Br	Br	-54.3 (0.1)	-54.6 (0.1)
6{3}	F	F	-48.1 (0.1)	-47.9 (0.1)
6{4}	H	H	-46.6 (0.1)	-44.9 (0.1)
6{5a}	Br	H	-49.6 (0.1)	-49.0 (0.1)
6{5b}	H	Br	-48.9 (0.1)	-47.3 (0.2)
6{6a}	F	H	-46.5 (0.1)	-41.6 (0.1)
6{6b}	H	F	-47.0 (0.1)	-47.2 (0.1)
6{7a}	F	Cl	-47.6 (0.1)	-46.3 (0.1)
6{7b}	Cl	F	-48.9 (0.1)	-49.5 (0.1)
6{8a}	H	CF ₃	-48.9 (0.1)	-46.4 (0.1)
6{8b}	CF ₃	H	-49.5 (0.1)	-45.3 (0.1)
6{9a}	F	Br	-49.9 (0.1)	-49.4 (0.1)
6{9b}	Br	F	-50.7 (0.1)	-49.4 (0.1)
6{10a}	F	CF ₃	-48.9 (0.1)	-48.0 (0.1)
6{10b}	CF ₃	F	-48.6 (0.1)	-45.8 (0.1)
6{11a}	F	OCH ₃	-50.6 (0.1)	-47.3 (0.2)
6{11b}	OCH ₃	F	-50.1 (0.1)	-44.8 (0.2)

2.3. Chemistry

As it is depicted in Scheme 1, the synthesis of compounds **6**{*x*} consists of a 6 steps route and the diversity of R^1 and R^2 was introduced at the beginning through the synthesis of the corresponding aryl acetate **8**{*x*}. All the synthesis of these starting materials and their corresponding 2-aryl acrylates **9**{*x*} by condensation of **8**{*x*} with paraformaldehyde in the presence of K_2CO_3 in DMF were described in a previous work⁴⁸. The 2-aryl acrylates **9**{*x*} were refluxed in MeOH with malononitrile (**10**) in the presence of NaOMe to afford through a Michael addition the corresponding pyridones **11**{*x*} in very good yields (up to 93%). Then, pyridones **11**{*x*} were condensed with phenyl guanidine (**12**) leading the corresponding intermediates **13**{*x*} which were transformed to the corresponding pyrido[2,3-*d*]pyrimidines **14**{*x*} through a Dimroth rearrangement upon treatment with NaOMe/MeOH under microwave irradiation at 140 °C during 40 min. To accomplish the dehydrogenation of compounds **14**{*x*}, different procedures were carried out depending on the substituents presents in R^1 and R^2 . When $R^1 = R^2 = Br$, **14**{2} was heated at 100 °C for 4h in anhydrous DMSO in presence of NaH to afford **15**{2}, whereas when $R^1 = F$ and $R^2 = CF_3$, **14**{10} was refluxed with activated MnO_2 in AcOH for 3h to yield **15**{10}. Finally, the desired compounds **6**{*x*} were obtained by methylation of the lactam nitrogen of the corresponding **15**{*x*} with MeI in DMSO in the presence of NaH, the yields being in the range 93–96%.



Scheme 1: Synthesis of pyrido[2,3-*d*]pyrimidines **6**{*x*}

2.4. Biological activity assessment

After their synthesis, compounds **6**{1}, **6**{2}, **6**{4} and **6**{10} were evaluated at Proqinase (<http://www.proqinase.com>) by measuring residual activity values (%) at a concentration of 10 μM in front of wild type EGFR. The results obtained (Table 2) indicate the best inhibition activity is for compound **6**{2} ($R^1 = R^2 = Br$) followed by compound **6**{1} ($R^1 = R^2 = Cl$) and finally the worst inhibitory activity is for **6**{10} ($R^1 = F$ and $R^2 = CF_3$), showing the following values of residual activity (% of control activity) 3%, 14% and 61%, respectively. These experimental inhibitory data are in good qualitative agreement with our calculations, showing that MM/GBSA calculations are useful for the purpose used in this work. These results would seem indicate that the bulkier the substituent R^1 and R^2 , the more active is the compound **6**{*x*}. This observation is supported by the almost inactivity observed for compound **6**{4} ($R^1 = R^2 = H$) but the required bulkiness has a limit as is clearly shown by compound **6**{10} ($R^1 = F$ and $R^2 = CF_3$).

Table 2. Residual activity values (%) at a concentration of 10 μ M of pyrido[2,3-*d*]pyrimidines **6{1}**, **6{2}**, **6{4}** and **6{10}** in front of EGFR wild type.

Structure	Residual activity (%)
6{1}	14
6{2}	3
6{4}	49
6{10}	61

2.5. Analysis of EGFR-**6{x}** interaction

Analysis of the RMSD for each of the ligands shows that the gly-rich loop, the activation loop, the α C helix and the DFG motif are stable throughout the simulation. Regarding oscillations around the average conformation, it was only observed that the gly-rich loop exhibits a larger RMSF in the case of ligand **6{10}** (see RMSF analysis in Supplementary Information).

In order to investigate the influence of the hydrogen bonding network on binding energies, the fraction of hydrogen bonding during the MD simulations was calculated with *cptraj* included in *AmberTools13*. The results are displayed in Table 3, where no substantial difference can be observed in those patterns.

Table 3. Donor and acceptor hydrogen bond atoms between ligands and EGFR residues through the last 10 ns of simulation. For distance cut-off and angular cut-off, values of 3.4 Å and 150° were selected, respectively. Average distances between heavy atoms (Å), and angles (°) are also shown. The values in parentheses represent the standard deviation. The two hydrogen atoms of NH₂ group are discriminated with apostrophe on one of them.

6{1}	Acceptor	Donor	Fraction	<Distance>	<Angle>
	N3	HN(Met793)	0.86	3.10 (0.16)	164.9 (9.6)
	Oγ1(Thr790)	HN(C4)	0.30	3.07 (0.15)	162.5 (7.0)
	O(Met793)	HN	0.30	2.93 (0.14)	156.8 (5.3)
	Oγ1(Thr790)	H'N(C4)	0.23	3.08 (0.15)	162.7 (7.0)
	O(Gln791)	H'N(C4)	0.02	2.89 (0.14)	154.1 (3.7)
6{2}	Acceptor	Donor	Fraction	<Distance>	<Angle>
	N3	HN(Met793)	0.79	3.09 (0.13)	164.1 (7.0)
	Oγ1(Thr790)	HN(C4)	0.72	2.97 (0.13)	163.0 (7.1)
	O(Met793)	HN	0.33	2.92 (0.14)	156.6 (5.1)
	O(Gln791)	H'N(C4)	0.08	2.91 (0.14)	154.5 (4.0)
	Oγ1(Thr790)	H'N(C4)	0.05	2.96 (0.13)	163.3 (7.7)
6{4}	Acceptor	Donor	Fraction	<Distance>	<Angle>
	N3	HN(Met793)	0.83	3.09 (0.14)	164.1 (7.0)
	O(Met793)	HN	0.37	2.91 (0.13)	157.7 (5.7)
	Oγ1(Thr790)	HN(C4)	0.23	3.07 (0.16)	162.7 (7.0)
	Oγ1(Thr790)	H'N(C4)	0.19	3.06 (0.15)	163.3 (7.2)
	N(Met793)	H'N(C4)	0.04	3.24 (0.11)	155.7 (5.0)
	O(Gln791)	HN(C4)	0.03	2.84 (0.12)	155.3 (4.3)
	O(Gln791)	H'N(H)	0.02	2.89 (0.14)	154.0 (4.1)
6{10a}	Acceptor	Donor	Fraction	<Distance>	<Angle>
	N3	HN(Met793)	0.81	3.12 (0.13)	164.1 (6.9)
	Oγ1(Thr790)	HN(C4)	0.46	3.09 (0.15)	163.9 (7.0)
	O(Met793)	HN	0.41	2.97 (0.15)	157.2 (5.3)
	Oγ1(Thr790)	H'N(C4)	0.24	3.08 (0.15)	163.7 (7.2)
	O(Gln791)	H'N(C4)	0.05	2.84 (0.12)	154.9 (4.1)
	O(Gln791)	HN(C4)	0.03	2.84 (0.12)	154.3 (4.0)

Decomposition of the binding energy and the van der Waals interaction between compounds and their neighboring residues are plotted in Figure 7. Overall, both plots follow a similar pattern in almost the entire range, which is consistent with the hypothesis that the van der Waals term has a predominant effect on the binding energy. Residues with the highest stabilizing contributions are Ala743, Lys745, Thr790, Met793, and Leu844, where the first three are close to the substituted aromatic ring A. The differences between the distances R¹...O(Ala743) and the van der Waals radii of the atoms involved are reported on Table 4. This magnitude increases in the order 6{2} < 6{1} < 6{10a} < 6{4}, what correlates with the loss of binding affinity. A similar effect is also observed between R¹ and the N atom of the adjacent residue Ile744. The linear correlation coefficients between components and binding energies shown in Table S1 confirm this trend.

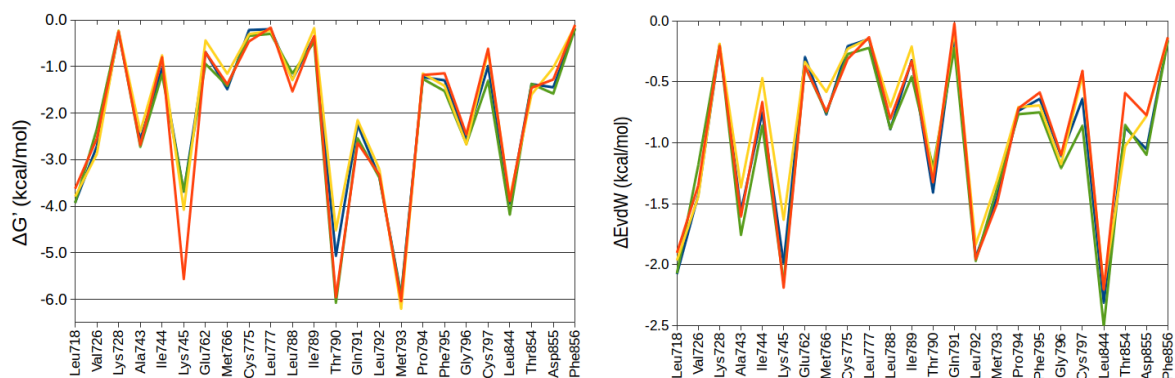


Figure 7. Decomposition of the binding energies $\Delta G'$ (left) and the van der Waals contribution ΔE_{vdw} (right) on a pairwise energy decomposition scheme for **6{1}** (blue), **6{2}** (green), **6{4}** (yellow), and **6{10a}** (red).

Table 4. Mean bond distance σ between R^1 substituent and the carbonyl oxygen of Ala743, standard deviation in parenthesis, and the difference δ between σ and the van der Waals radii of atoms involved [$\delta = \sigma - r_{vdw}(O) - r_{vdw}(R^1)$] (Distances in Å).

$R^1 \dots O(\text{Ala743})$	σ	δ
6{2} Br \cdots O	3.48 (0.21)	0.11
6{1} Cl \cdots O	3.46 (0.26)	0.19
6{10a} F \cdots O	3.28 (0.30)	0.29
6{4} H \cdots O	3.65 (0.41)	0.93

Analysis of water clusters on all four ligands shows a conserved O=C(7) interaction through hydrogen bonding with a water molecule. Water distribution around O=C(7) is similar for all ligands with the exception of the **6{10a}** complex, where the displacement of Lys745 restricts the available space. There are other two water molecules within the binding site interacting with Gln791 and Thr854, however, unlike the case of erlotinib^{43, 49}, these water molecules are not directly involved in hydrogen bonding between the ligand and EGFR. In the case of **6{1}** there is another water molecule at the bottom of the pocket, which interacts with Phe856.

3. Conclusions

Currently, most hit-to-lead campaigns are based on a “trial and error” approach. A computationally-aided synthetic approach is usually not undertaken. In this work we explored the use of a molecular dynamics-based end-point binding free energy protocol to estimate the relative affinities of a virtual combinatorial library designed around a 4-amino substituted pyridopyrimidine EGFR model inhibitor (**6{1}**) as a tool to guide chemical synthesis toward the most promising compounds, and then validate our predictions through biological activity evaluation.

It was observed that the experimental inhibition activity was in good qualitative agreement with our binding free energy calculations using the MM/GBSA method for the four synthesized compounds. From the MD trajectories, we concluded that differences at the binding free energy level are governed by van der Waals interaction, showing the compounds examined negligible differences in terms of hydrogen bonding, and water molecules bridging their interaction with EGFR. It should be also mentioned that a 6-dibromophenyl-substituted molecule which exhibited an enhanced affinity toward EGFR compared to the reference

ligand was obtained. Although further validation is needed on other molecular systems – since in many cases the usefulness of a given computational method is system-dependent-, we consider that this approach offers an attractive balance of performance and computational affordability.

4. Experimental section

4.1. Docking

Ligand **6{I}** was docked within the binding site of EGFR (PDB: 2ITW⁴²) using a flexible-ligand/rigid-receptor approach, as implemented in the ICM package^{50, 51}. Two dominant ligand binding modes were observed, and a representative complex of each was chosen, and subjected to a flexible-ligand/flexible-side chain Monte Carlo-based global energy optimization^{40, 52-55}. Solvation effects were taken into account using a Generalized Born model⁵⁶. A conformational stack was collected throughout the simulation of each complex⁵⁷, and the best-energy structure corresponding to each initial binding mode was kept, labeled as “favorable” and “unfavorable”, according to their relative energy.

4.2. Preparation of the molecular systems

The simulations were based on the X-ray crystal structure of EGFR in complex with (PDB: 2ITW)⁴². In the preparation of the receptor, all Asp and Glu residues were considered to have a negative charge and all the Arg and Lys residues were considered to have a positive charge. Histidine tautomers were assigned following the hydrogen bonding pattern. In the case of His835, close to binding site, was protonated on the N ϵ .

4.3. Molecular dynamics (MD) simulations

The complexes have a net charge of +1. To achieve electroneutrality, a chloride was added as counterion, with the Leap module. The neutralized complexes were immersed in a box of TIP3P⁵⁸ waters which extended up to 10 Å from the solute. The protein was described using the Amber99SB force field⁵⁹ with the dielectric constant taken as 1, while the ligands were described using the Generalized Amber Force Field (GAFF)⁶⁰, with charges derived from AM1-BCC⁶¹, which were calculated with the Antechamber module. Leap and Antechamber are included in the package *AmberTools* 13.0⁶².

All MD simulations were run using the *NAMD* 2.9 software⁶³. The van der Waals interaction cutoff distances were set at 12 Å and long-range electrostatic forces were computed using the particle mesh Ewald summation method with a grid size set to 1.0 Å. The 1-4 contributions were multiplied by a factor of 0.83 to match the *AMBER* force field requirements. For all production simulations, constant temperature (300 K) was maintained using Langevin dynamics with a damping coefficient of 5 ps⁻¹, while pressure was kept constant at 1 atm through the Nosé-Hoover Langevin piston method with a decay period of 200 fs and a damping time constant of 100 fs. A time step of 1 fs was used along molecular mechanics. Bonds involving hydrogen atoms were constrained using the SHAKE algorithm⁶⁴.

4.4. MM/GBSA calculations

Small-molecule-protein binding free energies were computed using the MM/GBSA method for all complexes, where the binding free energy is calculated as the difference between the bound and unbound states of protein and ligand, according to^{34, 65-68}

$$\begin{aligned}\Delta G_{bind} &= \Delta \langle E_{MM} \rangle + \Delta G_{solv} - T\Delta S_{bind} \\ &= \Delta G' - T\Delta S_{bind}\end{aligned}\quad (1)$$

where $\langle \dots \rangle$ is the trajectory average, E_{MM} is the gas-phase potential energy, and $\Delta G_{solv} = \Delta \langle W \rangle$ (W is the effective solvation energy which incorporates the solvent degrees of freedom). Provided the high similarity of the molecules on Table 1, the entropic changes upon binding were assumed constant, and thus $\Delta G'$ is reported on Table 1. The solvation free energy ΔG_{solv} was separated into polar and non-polar contributions as

$$\Delta G_{solv} = \Delta G_{solv}^{pol} + \Delta G_{solv}^{np} \quad (2)$$

The polar contribution to the solvation free energy was calculated using the generalized Born (GB) model⁶⁷ implemented in *MMPBSA.py* module of Amber⁶⁹, *igb=2* as selected model. The hydrophobic contribution to the solvation free energy (ΔG_{nonp}) was determined using the solvent-accessible surface area (SASA) as

$$G_{nonp} = \gamma \text{SASA} + \beta \quad (3)$$

where values for γ and β were set to $0.0072 \text{ kcal}\cdot\text{mol}^{-2}$ and $0 \text{ kcal}\cdot\text{mol}^{-1}$, respectively. The protein–ligand binding free energy was calculated using a single trajectory (for ligand, receptor and complex)^{34, 45} based on 1000 snapshots taken from the last 10 ns portion (10 ps interval) of the MD simulation trajectories.

For the purpose of obtaining the detailed representation of the ligands/EGFR interactions, free energy decomposition analysis was employed to decompose the total binding free energies into ligand–residue pairs. These calculations were performed using a pairwise energy decomposition scheme (idecomp option 3) also with the *MMPBSA.py* module. In this scheme, interactions are decomposed by specific residue pairs by including only those interactions in which one atom from each of the analyzed residues is participating, following the work of Gohlke et al.⁷⁰.

4.5. Synthesis and characterization of compounds

4.5.1. General

All solvents and chemicals were reagent grade. Unless otherwise mentioned, all solvents and chemicals were purchased from commercial vendors (Fluka, Aldrich, ABCR and ACROS Organics) and used without purification. Compound **6{I}** was prepared as previously described²⁶. ^1H and ^{13}C NMR spectra were recorded on a Varian 400-MR spectrometer that was operating at a field strength of 400 and 100.6 MHz, respectively. Chemical shifts were reported in parts per million (δ) and coupling constants (J) were in Hz by using, in the case of ^1H NMR spectroscopy, TMS as an internal standard, and in the case of ^{13}C NMR spectroscopy the solvent at 39.5 ppm (DMSO- d_6) or at 29.84 ppm (acetone- d_6) as an internal reference. Standard and peak multiplicities are designed as follows: s, singlet; d, doublet; t, triplet; q, quartet; br, broad signal. IR spectra were recorded in a Thermo Scientific Nicolet iS10 FTIR spectrophotometer with Smart iTr. Wavenumbers (ν) are expressed in cm^{-1} . MS data (m/z (%), EI, 70 eV) were obtained by using an Agilent Technologies 5975 spectrometer and a Hewlett Packard HP5988A quadrupole mass spectrometer operating in electronic ionization (EI) mode at 70 eV and at 4 kV accelerating potential, or a Bruker Biotoff II spectrometer operating in electrospray ionization (ESI) mode with a Time of Flight (TOF) detector or on a VG AutoSpec (Micromass Instruments). HRMS data were obtained by using a VG AutoSpec (Micromass Instruments) Trisector EBE high resolution spectrometer (EI mode), a Bruker Biotof II mass spectrometer (ESI TOF mode). Elemental microanalyses

were obtained on a EuroVector Instruments Euro EA elemental analyzer. The melting points were determined with a Büchi-Tottoli 530 capillary apparatus and are uncorrected.

Microwave irradiation experiments were carried out in a InitiatorTM (Biotage) microwave apparatus, operating at a frequency of 2.45 GHz with continuous irradiation power from 0 to 400 W. Reactions were carried out in 0.5, 2.5, 5, 20 mL glass tubes, sealed with aluminium/Teflon crimp tops, which can be exposed up to 250 °C and 20 bar internal pressure. Temperature was measured with an IR sensor on the outer surface of the process vial. After the irradiation period, the reaction vessel was cooled rapidly to 50 °C by air jet cooling.

The synthesized compounds have been checked for their melting points, physical nature, IR, ¹H NMR, ¹³C NMR, Mass spectroscopy and Elemental analysis for individual compounds and the data are summarized as under

4.5.2. 5-(2,6-dibromophenyl)-2-methoxy-6-oxo-1,4,5,6-tetrahydropyridine-3-carbonitrile (**11{2}**)

To a solution of 913.0 mg (16.42 mmol) of NaOMe in 20 mL of anhydrous methanol, 802.0 mg (12.14 mmol) of malononitrile (**10**) were added and the mixture left cool down. 3.26 g (10.2 mmol) of methyl 2-(2,6-dibromophenyl)acrylate (**9{2}**)⁴⁸ were added slowly and the mixture refluxed for 5 h. The solvent was evaporated *in vacuo* and the residue dissolved in the minimum quantity of water. Careful neutralization to pH 7 with 2M aqueous HCl allowed the precipitation of a solid which was filtered, washed with cold water and dried *in vacuo* over phosphorus pentoxide. 3.750 g (9.71 mmol, 95%) of 5-(2,6-dibromophenyl)-2-methoxy-6-oxo-1,4,5,6-tetrahydropyridine-3-carbonitrile (**11{2}**) were obtained as a white solid, mp 200-203 °C. ¹H NMR (400 MHz, DMSO-*d*₆) δ (ppm): 10.88 (br s, 1H), 7.71 (ddd, *J* = 16.1, 8.0, 1.0 Hz, 2H), 7.19 (t, *J* = 8.0 Hz, 1H), 4.71 (dd, *J* = 13.9, 8.8 Hz, 1H), 3.97 (s, 3H), 2.97 (dd, *J* = 15.2, 13.9 Hz, 1H), 2.46 (dd, *J* = 15.2, 8.8 Hz, 1H). ¹³C NMR (100.6 MHz, DMSO-*d*₆) δ (ppm): 169.0, 159.5, 136.5, 133.9, 132.3, 130.8, 126.5, 124.2, 118.3, 62.5, 59.1, 47.3, 25.1. IR (KBr): ν(cm⁻¹): 3230, 3183, 2926, 2203, 1713, 1645, 1487, 1254. MS (70 eV, EI): *m/z* (%) = 385.8 (19) [M]⁺, 304.9 (12) [M-Br]⁺, 275.7 (100) [M-CH₃OBr]⁺. HRMS (70 eV, EI): calcd. for C₁₃H₁₀Br₂N₂O₂: 383.9109 [M]⁺, found: 383.9109.

4.5.3. 2-methoxy-6-oxo-5-phenyl-1,4,5,6-tetrahydropyridine-3-carbonitrile (**11{4}**)

As above for **11{2}** but using NaOMe (1.289 g, 23.18 mmol), anhydrous methanol (29 mL), malononitrile (**10**) (1.133 g, 17.15 mmol) and methyl 2-phenylacrylate (**9{4}**)⁴⁸ (2.34 g, 14.4 mmol) to afford 1.741 g (7.63 mmol, 53%) of 2-methoxy-6-oxo-5-phenyl-1,4,5,6-tetrahydropyridine-3-carbonitrile (**11{4}**) as a yellow solid, mp 138-141 °C. ¹H NMR (400 MHz, DMSO-*d*₆) δ (ppm): 10.78 (br s, 1H), 7.37 – 7.32 (m, 2H), 7.31 – 7.27 (m, 1H), 7.26 – 7.23 (m, 2H), 3.95 (s, 3H), 3.85 (dd, *J* = 11.0, 6.7 Hz, 1H), 2.73 (dd, *J* = 15.4, 11.0 Hz, 1H), 2.60 (dd, *J* = 15.4, 6.7 Hz, 1H). ¹³C-RMN (100.6 MHz, DMSO-*d*₆) δ (ppm): 171.3, 159.7, 137.8, 128.37, 128.36, 127.1, 118.5, 63.2, 58.9, 45.5, 28.0. IR (KBr): ν(cm⁻¹): 3427, 3226, 2204, 1712, 1644. MS (ESI-TOF): *m/z* (%) = 229.1 (20) [M+H]⁺. HRMS (ESI-TOF): calcd. for C₁₃H₁₃N₂O₂: 229.0972 [M+H]⁺, found: 229.0969.

4.5.4. 5-(2-fluoro-6-(trifluoromethyl)phenyl)-2-methoxy-6-oxo-1,4,5,6-tetrahydropyridine-3-carbonitrile (**11{10}**)

As above for **11{2}** but using NaOMe (913.0 mg, 16.42 mmol), anhydrous methanol (20 mL), malononitrile (**10**) (802.0 mg, 12.14 mmol) and methyl 2-(2-fluoro-6-(trifluoromethyl)phenyl)acrylate (**9{10}**) (2.53 g, 10.2 mmol) to afford 2.969 g (9.45 mmol, 93%) of 5-(2-fluoro-6-(trifluoromethyl)phenyl)-2-methoxy-6-oxo-1,4,5,6-tetrahydropyridine-3-carbonitrile (**11{10}**) as a white solid, mp 207-208 °C. ¹H NMR (400 MHz, DMSO-*d*₆) δ

(ppm): 10.93 (br s, 1H), 7.67 – 7.57 (m, 3H), 4.14 (dd, $J = 13.8, 7.1$ Hz, 1H), 3.98 (s, 3H), 2.79 (t, $J = 15.0$ Hz, 1H), 2.43 (dd, $J = 15.3, 7.5$ Hz, 1H). ^{13}C NMR (100.6 MHz, DMSO- d_6) δ (ppm): 169.2, 161.0 (d, $J = 248.1$ Hz), 159.85, 130.4 (d, $J = 9.7$ Hz), 129.7 (dq, $J = 30.2, 5.6$ Hz), 124.3 (d, $J = 16.0$ Hz), 123.6 (dq, $J = 274.3, 3.6$ Hz), 121.9, 120.7 (d, $J = 22.6$ Hz), 118.2, 62.9, 59.0, 40.15, 26.6 (d, $J = 3.3$ Hz). IR (KBr): $\nu(\text{cm}^{-1})$: 3220, 3180, 2960, 2199, 1715, 1639, 1487, 1323, 1251, 1120. MS (70 eV, EI): m/z (%) = 314.0 (16) $[\text{M}]^+$, 204.0 (100) $[\text{M}-\text{C}_3\text{H}_3\text{F}_3\text{N}]^+$. HRMS (70 eV, EI): calcd. for $\text{C}_{14}\text{H}_{10}\text{F}_4\text{N}_2\text{O}_2$: 314.0678 $[\text{M}]^+$, found: 314.0680.

4.5.5. 2-amino-6-(2,6-dibromophenyl)-4-imino-3-phenyl-4,5,6,8-tetrahydropyrido[2,3-*d*]pyrimidin-7(3*H*)-one (13{2})

A mixture of *N*-phenylguanidine carbonate (**12** having a $\text{C}_7\text{H}_9\text{N}_3 \cdot (\text{H}_2\text{CO}_3)_{0.7}$ stoichiometry) (523.0 mg, 3.07 mmol of *N*-phenylguanidine), sodium methoxide (232.5 mg, 4.30 mmol), and 1,4-dioxane (15 mL) is sealed in a 20 mL microwave vial and heated at 65 °C under microwave irradiation for 15 min. A clear solution with a white precipitate is obtained. The solid is removed by filtration and the mother liquor is transferred to a 20 mL microwave vial together with 5-(2,6-dibromophenyl)-2-methoxy-6-oxo-1,4,5,6-tetrahydropyridine-3-carbonitrile (**11{2}**) (393.0 mg, 1.02 mmol). The vial is sealed and heated at 140 °C under microwave irradiation for 40 min. The solvent of the red solution obtained is removed *in vacuo*, and the resulting red oil is treated with acetone (10 mL) and sonication for 10 min while a white precipitate is formed. The solid is filtered, washed with cold acetone to afford 402.4 mg (3.29 mmol) (81%) of 2-amino-6-(2,6-dibromophenyl)-4-imino-3-phenyl-4,5,6,8-tetrahydropyrido[2,3-*d*]pyrimidin-7(3*H*)-one (**13{2}**) as a light orange solid, mp 262–264 °C. ^1H NMR (400 MHz, DMSO- d_6) δ (ppm): 10.00 (br s, 1H), 7.72 (dd, $J = 8.0, 1.1$ Hz, 1H), 7.69 (dd, $J = 8.0, 1.1$ Hz, 1H), 7.58 (t, $J = 7.5$ Hz, 2H), 7.55 – 7.48 (m, 1H), 7.32 (d, $J = 7.3$ Hz, 2H), 7.18 (t, $J = 8.0$ Hz, 1H), 6.19 (br s, 2H), 5.54 (br s, 1H), 4.62 (dd, $J = 13.3, 9.4$ Hz, 1H), 2.86 (dd, $J = 16.0, 9.4$ Hz, 1H), 2.74 (dd, $J = 15.9, 13.4$ Hz, 1H). ^{13}C NMR (100.6 MHz, DMSO- d_6) δ (ppm): 169.7, 156.3, 153.9, 149.0, 138.2, 135.3, 135.2, 133.8, 132.1, 130.5, 130.4, 129.5, 129.4, 129.1, 126.3, 124.3, 84.9, 47.9, 24.5. IR (KBr): $\nu(\text{cm}^{-1})$: 3396, 3174, 1685, 1634, 1525, 1486, 1430, 1379, 1315, 1268, 1198, 767, 703. Anal. calcd for $\text{C}_{19}\text{H}_{15}\text{N}_5\text{OBr}_2$: C: 46.65%, H: 3.09%, N: 14.32%, O: 3.27%, Br: 32.67%; Found: C: 46.49%, H: 2.99%, N: 14.23%. HRMS (ESI-TOF): calcd. for $\text{C}_{19}\text{H}_{16}\text{Br}_2\text{N}_5\text{O}$: 487.9716 $[\text{M}+\text{H}]^+$, found: 487.9718.

4.5.6. 2-amino-4-imino-3,6-diphenyl-4,5,6,8-tetrahydropyrido[2,3-*d*]pyrimidin-7(3*H*)-one (13{4})

As above for **13{2}** but using *N*-phenylguanidine carbonate (**12** having a $\text{C}_7\text{H}_9\text{N}_3 \cdot (\text{H}_2\text{CO}_3)_{0.7}$ stoichiometry) (523.0 mg, 3.07 mmol of *N*-phenylguanidine), sodium methoxide (232.5 mg, 4.30 mmol), dioxane (15 mL) and 2-methoxy-6-oxo-5-phenyl-1,4,5,6-tetrahydropyridine-3-carbonitrile (**11{4}**) (232.4 mg, 1.02 mmol) to afford 192.7 mg (0.58 mmol, 53%) of 2-amino-4-imino-3,6-diphenyl-4,5,6,8-tetrahydropyrido[2,3-*d*]pyrimidin-7(3*H*)-one (**13{4}**) as a white solid, mp 248–251 °C. ^1H NMR (400 MHz, DMSO- d_6) δ (ppm): 9.94 (br s, 1H), 7.63 – 7.46 (m, 3H), 7.38 – 7.18 (m, 7H), 6.11 (br s, 2H), 5.04 (br s, 1H), 3.80 (dd, $J = 9.4, 7.4$ Hz, 1H), 2.84 (dd, $J = 16.1, 7.3$ Hz, 1H), 2.69 (dd, $J = 15.9, 9.3$ Hz, 1H). ^{13}C NMR (100.6 MHz, DMSO- d_6) δ (ppm): 172.0, 153.7, 149.9, 139.7, 135.3, 130.5, 129.5, 129.3, 129.1, 128.2, 128.2, 126.7, 86.2, 46.1, 26.4. IR (KBr): $\nu(\text{cm}^{-1})$: 3491, 3412 3313, 3153, 2890, 1684, 1637, 1524, 1489, 1454, 1380, 1313, 1260, 1197, 770, 701. HRMS (ESI-TOF): calcd. For $\text{C}_{19}\text{H}_{18}\text{N}_5\text{O}$: 332.1506 $[\text{M}+\text{H}]^+$, found: 332.1514.

4.5.7. 2-amino-6-(2-fluoro-6-(trifluoromethyl)phenyl)-4-imino-3-phenyl-4,5,6,8-tetrahydropyrido[2,3-*d*]pyrimidin-7(3*H*)-one (13{10})

As above for 13{2} but using *N*-phenylguanidine carbonate (12 having a $C_7H_9N_3 \cdot (H_2CO_3)_{0.7}$ stoichiometry) (523.0 mg, 3.07 mmol of *N*-phenylguanidine), sodium methoxide (232.5 mg, 4.30 mmol), dioxane (15 mL) and 5-(2-fluoro-6-(trifluoromethyl)phenyl)-2-methoxy-6-oxo-1,4,5,6-tetrahydropyridine-3-carbonitrile (11{10}) (320.0 mg, 1.02 mmol) to afford 393.9 mg (0.94 mmol, 93%) of 2-amino-6-(2-fluoro-6-(trifluoromethyl)phenyl)-4-imino-3-phenyl-4,5,6,8-tetrahydropyrido[2,3-*d*]pyrimidin-7(3*H*)-one (13{10}) as a white solid, mp 252-254 °C. 1H NMR (400 MHz, DMSO-*d*₆) δ (ppm): 10.05 (br s, 1H), 7.70 – 7.45 (m, 6H), 7.31 (dd, *J* = 13.2, 7.5 Hz, 2H), 6.16 (br s, 2H), 5.27 (br s, 1H), 4.01 (dd, *J* = 13.8, 8.1 Hz, 1H), 2.92 (dd, *J* = 15.3, 8.2 Hz, 1H), 2.57 (dd, *J* = 15.0, 13.8 Hz, 1H). ^{13}C NMR (100.6 MHz, DMSO-*d*₆) δ (ppm): 169.7, 161.1 (d, *J* = 247.8 Hz), 156.0, 153.9, 149.7, 135.2, 130.6, 129.9 (d, *J* = 9.8 Hz), 129.7 (m), 129.5, 129.4 (m), 129.4, 129.2, 126.5 (d, *J* = 16.5 Hz), 123.7 (dq, *J* = 274.1, 3.2 Hz), 121.7 (m), 120.6 (d, *J* = 22.9 Hz), 85.7, 40.7, 25.8 (d, *J* = 2.6 Hz). IR (KBr): ν (cm⁻¹): 3446, 3312, 3177, 2944, 1689, 1643, 1523, 1468, 1384, 1318, 1267, 1167, 1120, 807. HRMS (ESI-TOF): calcd. for C₂₀H₁₆F₄N₅O: 418.1285 [M+H]⁺, found: 418.1300.

4.5.8. 4-amino-6-(2,6-dibromophenyl)-2-(phenylamino)-5,8-dihydropyrido[2,3-*d*]pyrimidin-7(6*H*)-one (14{2})

A mixture of 2-amino-6-(2,6-dibromophenyl)-4-imino-3-phenyl-4,5,6,8-tetrahydropyrido[2,3-*d*]pyrimidin-7(3*H*)-one (13{2}) (1.609 g, 3.29 mmol), sodium methoxide (177.7 mg, 3.29 mmol) and methanol (10 mL) is sealed in a 20 mL microwave vial and heated at 140 °C under microwave irradiation for 40 min. The white solid obtained is filtered, washed with water, ethanol and diethyl ether to afford 1.429 mg (2.92 mmol) (89%) of pure 4-amino-6-(2,6-dibromophenyl)-2-(phenylamino)-5,8-dihydropyrido[2,3-*d*]pyrimidin-7(6*H*)-one (14{2}), mp > 280 °C. 1H NMR (400 MHz, DMSO-*d*₆) δ (ppm): 10.35 (br s, 1H), 8.75 (br s, 1H), 7.84 (dd, *J* = 8.7, 1.0 Hz, 2H), 7.73 (ddd, *J* = 12.6, 8.0, 1.2 Hz, 2H), 7.23 – 7.15 (m, 3H), 6.84 (tt, *J* = 7.3, 1.1 Hz, 1H), 6.39 (br s, 2H), 4.70 (dd, *J* = 13.0, 9.2 Hz, 1H), 2.96 (dd, *J* = 15.9, 9.2 Hz, 1H), 2.85 (dd, *J* = 15.9, 13.0 Hz, 1H). ^{13}C NMR (100.6 MHz, DMSO-*d*₆) δ (ppm): 169.2, 161.5, 158.3, 155.6, 141.4, 138.2, 133.9, 132.1, 130.5, 128.2, 126.3, 124.4, 120.2, 118.4, 84.1, 47.9, 23.7. IR (KBr): ν (cm⁻¹): 3499, 3400, 3286, 3201, 3136, 3090, 2917, 1676, 1637, 1612, 1574, 1550, 1499, 1478, 1441, 1382, 1246, 778, 757. Anal. calcd for C₁₉H₁₅N₅OBr₂: C: 46.65%, H: 3.09%, N: 14.32%, O: 3.27%, Br: 32.67%; Found: C: 46.67%, H: 2.90%, N: 14.18%. HRMS (ESI-TOF): calcd. for C₁₉H₁₆Br₂N₅O: 487.9716 [M+H]⁺, found: 487.9713.

4.5.9. 4-amino-6-phenyl-2-(phenylamino)-5,8-dihydropyrido[2,3-*d*]pyrimidin-7(6*H*)-one (14{4})

As above for 14{2} but using 2-amino-4-imino-3,6-diphenyl-4,5,6,8-tetrahydropyrido[2,3-*d*]pyrimidin-7(3*H*)-one (13{4}) (497.1 mg, 1.5 mmol), sodium methoxide (81.0 mg, 1.5 mmol) and methanol (5 mL) to afford 416.0 mg (1.26 mmol, 84%) of pure 4-amino-6-phenyl-2-(phenylamino)-5,8-dihydropyrido[2,3-*d*]pyrimidin-7(6*H*)-one (14{4}) as a white solid, mp > 280 °C. 1H NMR (400 MHz, DMSO-*d*₆) δ (ppm): 10.27 (br s, 1H), 8.72 (br s, 1H), 7.83 (d, *J* = 7.7 Hz, 2H), 7.36 – 7.29 (m, 2H), 7.29 – 7.22 (m, 3H), 7.18 (t, *J* = 7.5 Hz, 2H), 6.84 (t, *J* = 7.3 Hz, 1H), 6.38 (br s, 2H), 3.87 (dd, *J* = 9.3, 7.0 Hz, 1H), 2.95 (dd, *J* = 15.9, 6.9 Hz, 1H), 2.82 (dd, *J* = 15.9, 9.5 Hz, 1H). ^{13}C NMR (100.6 MHz, DMSO-*d*₆) δ (ppm): 172.0, 161.3, 158.2, 156.1, 141.5, 139.6, 128.3, 128.2, 128.2, 126.8, 120.2, 118.4, 85.7, 46.2, 25.6. IR (KBr): ν (cm⁻¹): 3469, 3255, 3171, 2926, 1696, 1642, 1591,

1574, 1542, 1485, 1449, 1433, 1379, 1243, 783, 785, 700. HRMS (ESI-TOF): calcd. for $C_{19}H_{18}N_5O$: 332.1506 $[M+H]^+$, found: 332.1508.

4.5.10. 4-amino-6-(2-fluoro-6-(trifluoromethyl)phenyl)-2-(phenylamino)-5,8-dihydropyrido[2,3-*d*]pyrimidin-7(6*H*)-one (**14{10}**)

As above for **14{2}** but using 2-amino-6-(2-fluoro-6-(trifluoromethyl)phenyl)-4-imino-3-phenyl-4,5,6,8-tetrahydropyrido[2,3-*d*]pyrimidin-7(3*H*)-one (**13{10}**) (1.576 g, 3.78 mmol), sodium methoxide (203.9 mg, 3.78 mmol) and methanol (10 mL) to afford 1.261 g (3.02 mmol, 80%) of pure 4-amino-6-(2-fluoro-6-(trifluoromethyl)phenyl)-2-(phenylamino)-5,8-dihydropyrido[2,3-*d*]pyrimidin-7(6*H*)-one (**14{10}**) as a white solid, mp > 280 °C. 1H NMR (400 MHz, DMSO-*d*₆) δ (ppm): 10.45 (br s, 1H), 8.78 (br s, 1H), 7.90 – 7.78 (m, 2H), 7.72 – 7.58 (m, 3H), 7.26 – 7.14 (m, 2H), 6.85 (tt, J = 7.5, 1.1 Hz, 1H), 6.42 (br s, 2H), 4.09 (dd, J = 13.6, 7.7 Hz, 1H), 3.02 (dd, J = 16.3, 7.7 Hz, 1H), 2.68 (t, J = 14.8 Hz, 1H). ^{13}C NMR (100.6 MHz, DMSO-*d*₆) δ (ppm): 169.5, 161.21, 161.18 (d, J = 248.0 Hz), 158.4, 155.9, 141.4, 130.0 (d, J = 9.7 Hz), 129.6 (dq, J = 29.5, 5.2 Hz), 128.22, 126.2 (d, J = 15.5 Hz), 123.7 (dq, J = 274.2, 3.5 Hz), 121.7, 120.6 (d, J = 22.3 Hz), 120.3, 118.5, 84.9, 40.7, 24.9 (d, J = 2.5 Hz). IR (KBr): ν (cm⁻¹): 3472, 3249, 3204, 3119, 2934, 1692, 1640, 1589, 1573, 1545, 1497, 1468, 1434, 1386, 1320, 1256, 1112, 784. Anal. calcd for $C_{20}H_{15}N_5OF_4$: C: 57.56%, H: 3.62%, N: 16.78%, O: 3.83%, Br: 18.21%; Found: C: 57.43%, H: 3.84%, N: 16.64%. HRMS (ESI-TOF): calcd. for $C_{20}H_{16}F_4N_5O$: 418.1285 $[M+H]^+$, found: 418.1289.

4.5.11. 4-amino-6-(2,6-dibromophenyl)-2-(phenylamino)pyrido[2,3-*d*]pyrimidin-7(8*H*)-one (**15{2}**)

A mixture of 244.6 mg (0.5 mmol) of 4-amino-6-(2,6-dibromophenyl)-5,6-dihydro-2-(phenylamino)pyrido[2,3-*d*]pyrimidin-7(8*H*)-one (**14{2}**) and 60.0 mg (1.5 mmol) of sodium hydride (NaH) (60% dispersion in mineral oil) in 5 mL of anhydrous DMSO was heated for 4 hours at 100 °C protected from moisture. The resulting solution was cooled down, water (300 mL) was added and it was neutralized with AcOH. The resulting precipitate was filtered, washed with EtOH and EtOEt and dried *in vacuo* over phosphorus pentoxide to afford 199.5 mg (0.41 mmol, 82%) of 4-amino-6-(2,6-dibromophenyl)-2-(phenylamino)pyrido[2,3-*d*]pyrimidin-7(8*H*)-one (**15{2}**) as a brownish solid, mp > 280 °C. 1H NMR (400 MHz, DMSO-*d*₆) δ (ppm): 11.85 (br s, 1H), 9.27 (br s, 1H), 8.00 (s, 1H), 7.90 (dd, J = 8.7, 1.0 Hz, 2H), 7.76 (d, J = 8.1 Hz, 2H), 7.31 (br s, 2H), 7.29 – 7.22 (m, 3H), 6.94 (t, J = 7.3 Hz, 1H). ^{13}C NMR (100.6 MHz, DMSO-*d*₆) δ (ppm): 161.1, 161.0, 159.5, 156.1, 140.6, 138.6, 135.0, 131.7, 131.0, 128.3, 126.0, 125.6, 121.4, 119.5, 91.2. IR (KBr): ν (cm⁻¹): 3396, 3207, 1626, 1594, 1529, 1498, 1446, 1310, 1261. HRMS (ESI-TOF): calcd. for $C_{19}H_{14}Br_2N_5O$: 485.9560 $[M+H]^+$, found: 485.9564.

4.5.12. 4-amino-6-phenyl-2-(phenylamino)pyrido[2,3-*d*]pyrimidin-7(8*H*)-one (**15{4}**)

As above for **15{2}** but using 4-amino-6-phenyl-2-(phenylamino)-5,8-dihydropyrido[2,3-*d*]pyrimidin-7(6*H*)-one (**14{4}**) (165.7 mg, 0.5 mmol), sodium hydride (NaH) (60% dispersion in mineral oil) (60.0 mg, 1.5 mmol) and anhydrous DMSO (5 mL) to afford 157.0 mg (0.48 mmol, 95%) of 4-amino-6-phenyl-2-(phenylamino)pyrido[2,3-*d*]pyrimidin-7(8*H*)-one (**15{4}**) as a brownish solid, mp > 280 °C. 1H NMR (400 MHz, DMSO-*d*₆) δ (ppm): 11.76 (br s, 1H), 9.22 (br s, 1H), 8.29 (s, 1H), 7.91 (dd, J = 8.7, 1.0 Hz, 2H), 7.75 (dd, J = 8.3, 1.3 Hz, 2H), 7.43 – 7.33 (m, 4H), 7.30 (tt, J = 7.4, 1.3 Hz, 1H), 7.27 – 7.21 (m, 2H), 6.94 (tt, J = 7.3, 1.1 Hz, 1H). ^{13}C NMR (100.6 MHz, DMSO-*d*₆) δ (ppm): 162.7, 161.1, 159.2, 155.3, 140.7, 136.6, 133.0, 128.3, 128.3, 127.8, 126.9, 124.1, 121.3, 119.4, 92.0. IR (KBr): ν (cm⁻¹): 3401, 3057, 2922, 1633, 1595, 1564, 1531, 1500, 1472, 1451, 1440, 1315, 1265, 899, 794, 752, 694. MS (ESI-TOF): m/z (%) = 330.1 (100) $[M+H]^+$, 313.1 (10) $[M-NH_2]^+$,

237.1 (1) $[M-NHPh]^+$. HRMS (ESI-TOF): calcd. for $C_{19}H_{16}N_5O$: 330.1349 $[M+H]^+$, found: 330.1349.

4.5.13. 4-amino-6-(2-fluoro-6-(trifluoromethyl)phenyl)-2-(phenylamino)pyrido[2,3-*d*]pyrimidin-7(8*H*)-one (15{10})

A mixture of 208.7 mg (0.5 mmol) of 4-amino-6-(2-fluoro-6-(trifluoromethyl)phenyl)-2-(phenylamino)-5,8-dihydropyrido[2,3-*d*]pyrimidin-7(6*H*)-one (14{10}) and 114.0 mg (1.0 mmol) of activated MnO_2 in 8.5 mL of acetic acid was refluxed for 3 hours. The resulting hot suspension was filtered and the solvent was removed *in vacuo*. The resulting solid was refluxed with water in order to eliminate MnO_2 traces, then filtrated and dried *in vacuo* over phosphorus pentoxide to afford 187.3 mg (0.45 mmol, 90%) of 4-amino-6-(2-fluoro-6-(trifluoromethyl)phenyl)-2-(phenylamino)pyrido[2,3-*d*]pyrimidin-7(8*H*)-one (15{10}) as a brownish solid, mp > 280 °C. 1H NMR (400 MHz, $DMSO-d_6$) δ (ppm): 11.85 (br s, 1H), 9.26 (br s, 1H), 8.07 (s, 1H), 7.89 (d, $J = 8.3$ Hz, 2H), 7.65 (m, 4H), 7.32 (br s, 2H), 7.25 (t, $J = 8.0$ Hz, 2H), 6.94 (t, $J = 7.2$ Hz, 1H). ^{13}C NMR (100.6 MHz, $DMSO-d_6$) δ (ppm): 161.8, 161.0, 160.5 (d, $J = 244.3$ Hz), 159.5, 156.2, 140.5, 135.4, 130.5 (d, $J = 8.9$ Hz), 130.4 (dq, $J = 31.2$, 3.0 Hz), 128.3, 123.9 (d, $J = 20.5$ Hz), 123.3 (dq, $J = 274.5$, 2.8 Hz), 121.9 (m), 121.4, 119.7, 119.5, 116.3, 91.0. IR (KBr): $\nu(cm^{-1})$: 3407, 3212, 1631, 1596, 1565, 1533, 1500, 1467, 1445, 1320, 1253, 1170, 1132, 902, 800. HRMS (ESI-TOF): calcd. for $C_{20}H_{14}F_4N_5O$: 416.1129 $[M+H]^+$, found: 416.1133.

4.5.14. 4-amino-6-(2,6-dibromophenyl)-8-methyl-2-(phenylamino)pyrido[2,3-*d*]pyrimidin-7(8*H*)-one (6{2})

To a solution of 341.0 mg (0.7 mmol) of 4-amino-6-(2,6-dibromophenyl)-2-(phenylamino)pyrido[2,3-*d*]pyrimidin-7(8*H*)-one (15{2}) in 10 mL of anhydrous $DMSO$, 28.0 mg (0.7 mmol) of sodium hydride (NaH) (60% dispersion in mineral oil) were added and the mixture was stirred for 1 hour at room temperature under nitrogen atmosphere. After this period, 43.8 μL (0.7 mmol) of methyl iodide were added dropwise and then stirred overnight at room temperature. The reaction was quenched by addition of 300 mL of water and the resulting precipitate was filtered, washed with water and dried *in vacuo* over phosphorus pentoxide to afford 325.0 mg (0.65 mmol, 93%) of 4-amino-6-(2,6-dibromophenyl)-8-methyl-2-(phenylamino)pyrido[2,3-*d*]pyrimidin-7(8*H*)-one (6{2}) as a brownish solid, mp 259-261 °C. 1H NMR (400 MHz, $DMSO-d_6$) δ (ppm): 9.43 (br s, 1H), 8.05 (s, 1H), 7.84 (d, $J = 8.5$ Hz, 2H), 7.77 (dd, $J = 8.0$, 0.7 Hz, 2H), 7.40 (br s, 2H), 7.35 – 7.23 (m, 3H), 7.01 – 6.92 (m, 1H), 3.60 (s, 3H). ^{13}C NMR (100.6 MHz, $DMSO-d_6$) δ (ppm): 161.7, 160.3, 159.0, 156.0, 140.4, 138.9, 133.6, 131.7, 131.0, 128.4, 125.6, 124.6, 121.7, 119.6, 91.6, 28.4. IR (KBr): $\nu(cm^{-1})$: 3402, 2924, 1631, 1572, 1523, 1496, 1468, 1445, 1344, 1315, 1193, 799. HRMS (ESI-TOF): calcd. for $C_{20}H_{16}Br_2N_5O$: 499.9716 $[M+H]^+$, found: 499.9717.

4.5.15. 4-amino-8-methyl-6-phenyl-2-(phenylamino)pyrido[2,3-*d*]pyrimidine-7(8*H*)-one (6{4})

As above for 6{2} but using 4-amino-6-phenyl-2-(phenylamino)pyrido[2,3-*d*]pyrimidin-7(8*H*)-one (15{4}) (164.7 mg, 0.5 mmol), sodium hydride (NaH) (60% dispersion in mineral oil) (20.0 mg, 0.5 mmol), anhydrous $DMSO$ (7 mL) and methyl iodide (31.3 μL , 0.5 mmol) to afford 143.7 mg (0.42 mmol, 84%) of 4-amino-8-methyl-6-phenyl-2-(phenylamino)pyrido[2,3-*d*]pyrimidine-7(8*H*)-one (6{4}) as a brownish solid, mp 238-241 °C. 1H NMR (400 MHz, $DMSO-d_6$) δ (ppm): 9.36 (br s, 1H), 8.30 (s, 1H), 7.84 (d, $J = 7.7$ Hz, 2H), 7.72 (dd, $J = 8.5$, 1.2 Hz, 2H), 7.44 (br s, 2H), 7.41 (t, $J = 7.6$ Hz, 2H), 7.34 – 7.24 (m, 3H), 6.96 (t, $J = 7.3$ Hz, 1H), 3.63 (s, 3H). ^{13}C NMR (100.6 MHz, $DMSO-d_6$) δ (ppm):

161.9, 161.7, 158.8, 155.4, 140.5, 137.1, 131.5, 128.6, 128.5, 127.9, 127.0, 123.0, 121.6, 119.5, 92.4, 28.5. IR (KBr): $\nu(\text{cm}^{-1})$: 3347, 3210, 3055, 2924, 1632, 1575, 1525, 1495, 1438, 1400, 1346, 1310, 1234, 1198, 1013, 797, 751, 696. HRMS (ESI-TOF): calcd for $\text{C}_{20}\text{H}_{18}\text{N}_5\text{O}$: 344.1506, $[\text{M}+\text{H}]^+$, found: 344.1508.

4.5.16. 4-amino-6-(2-fluoro-6-(trifluoromethyl)phenyl)-8-methyl-2-(phenylamino)pyrido[2,3-*d*]pyrimidine-7(8*H*)-one (6{10})

As above for 6{2} but using 4-amino-6-(2-fluoro-6-(trifluoromethyl)phenyl)-2-(phenylamino)pyrido[2,3-*d*]pyrimidin-7(8*H*)-one (15{10}) (290.7 mg, 0.7 mmol), sodium hydride (NaH) (60% dispersion in mineral oil) (28.0 mg, 0.7 mmol), anhydrous DMSO (10 mL) and methyl iodide (43.8 μL , 0.7 mmol) to afford 283.2 mg (0.66 mmol, 95%) of 4-amino-6-(2-fluoro-6-(trifluoromethyl)phenyl)-8-methyl-2-(phenylamino)pyrido[2,3-*d*]pyrimidine-7(8*H*)-one (6{10}) as a brownish solid, mp 260-261 °C. ^1H NMR (400 MHz, acetone-*d*₆) δ (ppm): 8.59 (br s, 1H), 7.99 (s, 1H), 7.91 (dd, $J = 8.7, 1.0$ Hz, 2H), 7.68 – 7.64 (m, 2H), 7.55 – 7.47 (m, 1H), 7.36 – 7.29 (m, 2H), 7.04 – 6.99 (m, 1H), 6.88 (br s 2H), 3.67 (s, 3H). ^{13}C NMR (100.6 MHz, acetone-*d*₆) δ (ppm): 163.0, 162.2, 162.1 (d, $J = 245.5$ Hz), 160.46, 157.73, 141.32, 134.02, 132.2 (dq, $J = 29.8, 3.1$ Hz), 131.1 (d, $J = 9.0$ Hz), 129.37, 125.6 (dq, $J = 20.7, 1.9$ Hz), 124.6 (qd, $J = 273.8, 3.6$ Hz), 122.9, 122.6 (m), 120.6, 120.1 (dd, $J = 23.4, 0.7$ Hz), 117.4, 92.5, 28.8. IR (KBr): $\nu(\text{cm}^{-1})$: 3350, 3206, 1633, 1611, 1573, 1523, 1469, 1442, 1320, 1169, 1134, 901, 800. Anal. calcd for $\text{C}_{21}\text{H}_{15}\text{N}_5\text{OF}_4$: C: 58.74%, H: 3.52%, N: 16.31%, O: 3.73%, F: 17.70%; Found: C: 58.72%, H: 3.47%, N: 16.00%. MS (70 eV, EI): m/z (%) = 429.1 (100) $[\text{M}]^+$, 410.1 (15) $[\text{M}-\text{F}]^+$, 360.1 (60) $[\text{M}-\text{CF}_3]^+$.

4.6. Enzymatic assay

The kinase inhibition profile of compounds was evaluated at ProQinase (<http://www.proqinase.com>) by measuring residual activity values at a concentration of 10 μM of the test compound in singlicate in front of EGFR wild type using the following protocol: The compounds were dissolved to 1×10^{-3} M stock solutions in 100% DMSO. Subsequently, 100 μL of each stock solution were transferred into wells A3-F12 of a microtiter plate (“master plate”). Wells A1-F2 were filled with 100 μL 100% DMSO as controls. 5 x 10 μL of the master plate were aliquoted into 5 copy plates, which were stored at -20 °C until use. For the testing of each group of up to 8 kinases, one copy plate was used. In the process, 90 μL H_2O were added to each well of a copy plate. To minimize precipitation, the H_2O was added to each well only a few minutes before the transfer of the compound solutions into the assay plates. The plate was shaken thoroughly, resulting in a “compound dilution plate” with a compound concentration of 1×10^{-4} M/10% DMSO. This plate was used for the transfer of 5 μL compound solution into the assay plates. The final volume of the assay was 50 μL . All compounds were tested at 1×10^{-5} M in singlicate. The final DMSO concentration in the reaction cocktails was 1% in all cases. The compound dilution plates were disposed at the end of each working day.

A radiometric protein kinase assay (^{33}P PanQinase® Activity Assay) was used for measuring the kinase activity of the corresponding protein kinases. All kinase assays were performed in 96-well FlashPlates™ from Perkin Elmer (Boston, MA, USA) in a 50 μL reaction volume. The reaction cocktail was pipetted in 4 steps in the following order: 10 μL of non-radioactive ATP solution (in H_2O); 25 μL of assay buffer/ $[\gamma\text{-}^{33}\text{P}]\text{-ATP}$ mixture; 5 μL of test sample in 10% DMSO; 10 μL of enzyme/substrate mixture. The assay for all protein kinases contained 70 mM HEPES-NaOH pH 7.5, 3 mM MgCl_2 , 3 mM MnCl_2 , 3 μM Na-orthovanadate, 1.2 mM DTT, ATP (variable amounts, corresponding to the apparent ATP-Km

of the respective kinase), [γ - ^{33}P]-ATP (approx. 8×10^5 cpm per well), protein kinase (variable amounts), and substrate (variable amounts). The protein kinase reaction cocktails were incubated at 30 °C for 60 min. The reaction was stopped with 50 μL of 2% (v/v) H_3PO_4 , plates were aspirated and washed two times with 200 μL 0.9% (w/v) NaCl. All assays were performed with a BeckmanCoulter Biomek 2000/SL robotic system. Incorporation of ^{33}P (counting of “cpm”) was determined with a microplate scintillation counter (Microbeta,Wallac). All protein kinase assays were performed with a BeckmanCoulter Core robotic system. For each kinase, the median value of the cpm of six wells of column 1 of each assay plate was defined as “low control” ($n = 6$). This value reflects unspecific binding of radioactivity to the plate in the absence of a protein kinase but in the presence of the substrate. Additionally, for each kinase the median value of the cpm of six wells of column 2 of each assay plate was taken as the “high control”, i.e. full activity in the absence of any inhibitor ($n = 6$). The difference between high and low control of each enzyme was taken as 100% activity. As part of the data evaluation the low control of each kinase was subtracted from the high control value as well as from their corresponding “compound values”. The residual activity (in %) for each compound well was calculated by using the following formula:

$$\text{Res. Activity (\%)} = 100 \times [(\text{signal of compound} - \text{low control}) / (\text{high control} - \text{low control})] \quad (4)$$

As a parameter for assay quality, the Z' -factor⁷¹ for the low and high controls of each assay plate ($n = 8$) was used. ProQinase's criterion for repetition of an assay plate is a Z' -factor below 0.4⁷². Z' -factors did not drop below 0.51, indicating an excellent assay quality.

Supporting Information. Backbone RMSD of EGFR in complex with the favorable pose of **6**{1}; RSMF plots of **6**{1}, **6**{2}, **6**{4}, and **6**{10a} complexes; interactions of **6**{1}, **6**{2}, **6**{4}, and **6**{10a} with EGFR; Linear correlation coefficients between these energy contributions and calculated binding free energies. Spectral data for new compounds **11**{x}, **13**{x}, **14**{x}, **15**{x} and **6**{x}.

Acknowledgments

We acknowledge the Centro de Computación de Alto Rendimiento (CeCAR) for providing computational time. This work has been supported by the Agencia Nacional de Promoción Científica y Tecnológica, Argentina (PICT-2011-2778 to CNC) and FOCER-Mercosur (COF 03/11). CNC thanks Molsoft LLC for providing an academic license for the ICM program. MJL is an Argentine National Research Council (CONICET) postdoctoral fellow.

References

1. Yarden, Y.; Sliwkowski, M. X. *Nat. Rev. Mol. Cell Biol.* **2001**, 2, 127.
2. Jardines, L.; Weiss, M.; Fowble, B.; Greene, M. *Pathobiology* **1993**, 61, 268.
3. Lupu, R.; Lippman, M. E. *Breast Cancer Res. Treat.* **1993**, 27, 83.
4. Fontana, X.; Ferrari, P.; Namer, M.; Peysson, R.; Salanon, C.; Bussiere, F. *Anticancer Res.* **1994**, 14, 2099.
5. Hickey, K.; Grehan, D.; Reid, I. M.; O'Briain, S.; Walsh, T. N.; Hennessy, T. P. *Cancer* **1994**, 74, 1693.
6. Stanton, P.; Richards, S.; Reeves, J.; Nikolic, M.; Edington, K.; Clark, L.; Robertson, G.; Souter, D.; Mitchell, R.; Hendler, F. J.; et al. *Br. J. Cancer* **1994**, 70, 427.
7. Sharma, S. V.; Bell, D. W.; Settleman, J.; Haber, D. A. *Nat. Rev. Cancer* **2007**, 7, 169.
8. Vivanco, I.; Robins, H. I.; Rohle, D.; Campos, C.; Grommes, C.; Nghiemphu, P. L.; Kubek, S.; Oldrini, B.; Chheda, M. G.; Yannuzzi, N.; Tao, H.; Zhu, S.; Iwanami, A.; Kuga,

- D.; Dang, J.; Pedraza, A.; Brennan, C. W.; Heguy, A.; Liau, L. M.; Lieberman, F.; Yung, W. K.; Gilbert, M. R.; Reardon, D. A.; Drappatz, J.; Wen, P. Y.; Lamborn, K. R.; Chang, S. M.; Prados, M. D.; Fine, H. A.; Horvath, S.; Wu, N.; Lassman, A. B.; DeAngelis, L. M.; Yong, W. H.; Kuhn, J. G.; Mischel, P. S.; Mehta, M. P.; Cloughesy, T. F.; Mellingshoff, I. K. *Cancer Discov.* **2012**, *2*, 458.
9. Normanno, N.; Bianco, C.; Strizzi, L.; Mancino, M.; Maiello, M. R.; De Luca, A.; Caponigro, F.; Salomon, D. S. *Curr. Drug Targets* **2005**, *6*, 243.
10. Harari, P. M. *Endocr. Relat. Cancer* **2004**, *11*, 689.
11. Messersmith, W. A.; Ahnen, D. J. *N. Engl. J. Med.* **2008**, *359*, 1834.
12. Wakeling, A. E.; Guy, S. P.; Woodburn, J. R.; Ashton, S. E.; Curry, B. J.; Barker, A. J.; Gibson, K. H. *Cancer Res.* **2002**, *62*, 5749.
13. Pollack, V. A.; Savage, D. M.; Baker, D. A.; Tsaparikos, K. E.; Sloan, D. E.; Moyer, J. D.; Barbacci, E. G.; Pustilnik, L. R.; Smolarek, T. A.; Davis, J. A.; Vaidya, M. P.; Arnold, L. D.; Doty, J. L.; Iwata, K. K.; Morin, M. J. *J. Pharmacol. Exp. Ther.* **1999**, *291*, 739.
14. Pao, W.; Miller, V.; Zakowski, M.; Doherty, J.; Politi, K.; Sarkaria, I.; Singh, B.; Heelan, R.; Rusch, V.; Fulton, L.; Mardis, E.; Kupfer, D.; Wilson, R.; Kris, M.; Varmus, H. *Proc. Natl. Acad. Sci. U. S. A.* **2004**, *101*, 13306.
15. Rusnak, D. W.; Lackey, K.; Affleck, K.; Wood, E. R.; Alligood, K. J.; Rhodes, N.; Keith, B. R.; Murray, D. M.; Knight, W. B.; Mullin, R. J.; Gilmer, T. M. *Mol. Cancer Ther.* **2001**, *1*, 85.
16. Lynch, T. J.; Bell, D. W.; Sordella, R.; Gurubhagavatula, S.; Okimoto, R. A.; Brannigan, B. W.; Harris, P. L.; Haserlat, S. M.; Supko, J. G.; Haluska, F. G.; Louis, D. N.; Christiani, D. C.; Settleman, J.; Haber, D. A. *N. Engl. J. Med.* **2004**, *350*, 2129.
17. Paez, J. G.; Janne, P. A.; Lee, J. C.; Tracy, S.; Greulich, H.; Gabriel, S.; Herman, P.; Kaye, F. J.; Lindeman, N.; Boggon, T. J.; Naoki, K.; Sasaki, H.; Fujii, Y.; Eck, M. J.; Sellers, W. R.; Johnson, B. E.; Meyerson, M. *Science* **2004**, *304*, 1497.
18. Barkovich, K. J.; Hariono, S.; Garske, A. L.; Zhang, J.; Blair, J. A.; Fan, Q. W.; Shokat, K. M.; Nicolaides, T.; Weiss, W. A. *Cancer Discov.* **2012**, *2*, 450.
19. Park, J. H.; Lemmon, M. A. *Cancer Discov.* **2012**, *2*, 398.
20. Blundell, T. L.; Patel, S. *Curr. Opin. Pharmacol.* **2004**, *4*, 490.
21. Boschelli, D. H.; Wu, Z.; Klutchko, S. R.; Showalter, H. D.; Hamby, J. M.; Lu, G. H.; Major, T. C.; Dahring, T. K.; Batley, B.; Panek, R. L.; Keiser, J.; Hartl, B. G.; Kraker, A. J.; Klohs, W. D.; Roberts, B. J.; Patmore, S.; Elliott, W. L.; Steinkampf, R.; Bradford, L. A.; Hallak, H.; Doherty, A. M. *Journal of medicinal chemistry* **1998**, *41*, 4365.
22. Hamby, J. M.; Connolly, C. J.; Schroeder, M. C.; Winters, R. T.; Showalter, H. D.; Panek, R. L.; Major, T. C.; Olsewski, B.; Ryan, M. J.; Dahring, T.; Lu, G. H.; Keiser, J.; Amar, A.; Shen, C.; Kraker, A. J.; Slintak, V.; Nelson, J. M.; Fry, D. W.; Bradford, L.; Hallak, H.; Doherty, A. M. *J. Med. Chem.* **1997**, *40*, 2296.
23. Klutchko, S. R.; Hamby, J. M.; Boschelli, D. H.; Wu, Z.; Kraker, A. J.; Amar, A. M.; Hartl, B. G.; Shen, C.; Klohs, W. D.; Steinkampf, R. W.; Driscoll, D. L.; Nelson, J. M.; Elliott, W. L.; Roberts, B. J.; Stoner, C. L.; Vincent, P. W.; Dykes, D. J.; Panek, R. L.; Lu, G. H.; Major, T. C.; Dahring, T. K.; Hallak, H.; Bradford, L. A.; Showalter, H. D.; Doherty, A. M. *J. Med. Chem.* **1998**, *41*, 3276.
24. Galve, I.; Puig de la Bellacasa, R.; Sanchez-Garcia, D.; Batllori, X.; Teixidó, J.; Borrell, J. I. *Mol. Divers.* **2012**, *16*, 639.
25. Perez-Pi, I.; Berzosa, X.; Galve, I.; Teixidó, J.; Borrell, J. I. *Heterocycles* **2010**, *82*, 581.
26. Puig de la Bellacasa, R.; Roue, G.; Balsas, P.; Perez-Galan, P.; Teixidó, J.; Colomer, D.; Borrell, J. I. *Eur. J. Med. Chem.* **2014**, *86*, 664.
27. Phatak, S. S.; Stephan, C. C.; Cavasotto, C. N. *Exp. Opin. Drug Discov.* **2009**, *4*, 947.

28. Jorgensen, W. L. *Acc. Chem. Res.* **2009**, *42*, 724.
29. Cavasotto, C. N. *Curr. Top. Med. Chem.* **2011**, *11*, 1528.
30. Jorgensen, W. L. *Angew. Chem. Int. Ed. Engl.* **2012**, *51*, 11680.
31. Cavasotto, C. N.; Orry, A. J. *Curr. Top. Med. Chem.* **2007**, *7*, 1006.
32. Guimaraes, C. R.; Cardozo, M. *J. Chem. Inf. Model.* **2008**, *48*, 958.
33. Thompson, D. C.; Humblet, C.; Joseph-McCarthy, D. *J. Chem. Inf. Model.* **2008**, *48*, 1081.
34. Anisimov, V. M.; Cavasotto, C. N. *J. Comput. Chem.* **2011**, *32*, 2254.
35. Ferrari, A. M.; Degliesposti, G.; Sgobba, M.; Rastelli, G. *Bioorg. Med. Chem.* **2007**, *15*, 7865.
36. Genheden, S.; Ryde, U. *J. Chem. Theory Comput.* **2011**, *7*, 3768.
37. Hou, T.; Wang, J.; Li, Y.; Wang, W. *J. Chem. Inf. Model.* **2011**, *51*, 69.
38. Spyraakis, F.; Cavasotto, C. N. *Arch. Biochem. Biophys.* **2015**, *583*, 105.
39. Diaz, P.; Phatak, S. S.; Xu, J.; Fronczek, F. R.; Astruc-Diaz, F.; Thompson, C. M.; Cavasotto, C. N.; Naguib, M. *ChemMedChem* **2009**, *4*, 1615.
40. Petrov, R. R.; Knight, L.; Chen, S. R.; Wager-Miller, J.; McDaniel, S. W.; Diaz, F.; Barth, F.; Pan, H. L.; Mackie, K.; Cavasotto, C. N.; Diaz, P. *Eur. J. Med. Chem.* **2013**, *69*, 881.
41. Phatak, S. S.; Gatica, E. A.; Cavasotto, C. N. *J. Chem. Inf. Model.* **2010**, *50*, 2119.
42. Yun, C. H.; Boggon, T. J.; Li, Y.; Woo, M. S.; Greulich, H.; Meyerson, M.; Eck, M. J. *Cancer Cell* **2007**, *11*, 217.
43. Stamos, J.; Sliwkowski, M. X.; Eigenbrot, C. *J. Biol. Chem.* **2002**, *277*, 46265.
44. Cavasotto, C. N.; Ortiz, M. A.; Abagyan, R. A.; Piedrafita, F. J. *Bioorg. Med. Chem. Lett.* **2006**, *16*, 1969.
45. Anisimov, V. M.; Ziemys, A.; Kizhake, S.; Yuan, Z.; Natarajan, A.; Cavasotto, C. N. *J. Comput. Aided Mol. Des.* **2011**, *25*, 1071.
46. Rastelli, G.; Del Rio, A.; Degliesposti, G.; Sgobba, M. *J. Comput. Chem.* **2010**, *31*, 797.
47. Pereira, E. G.; Moreira, M. A.; Caffarena, E. R. *J. Mol. Model.* **2012**, *18*, 4333.
48. Camarasa, M.; Barnils, C.; Puig de la Bellacasa, R.; Teixidó, J.; Borrell, J. I. *Mol. Divers.* **2013**, *17*, 525.
49. Park, J. H.; Liu, Y.; Lemmon, M. A.; Radhakrishnan, R. *Biochem. J.* **2012**, *448*, 417.
50. Abagyan, R.; Totrov, M.; Kuznetsov, D. *J. Comput. Chem.* **1994**, *15*, 488.
51. ICM. MolSoft, LLC: La Jolla, CA, 2012.
52. Monti, M. C.; Casapullo, A.; Cavasotto, C. N.; Tosco, A.; Dal Piaz, F.; Ziemys, A.; Margarucci, L.; Riccio, R. *Chem.-Eur. J.* **2009**, *15*, 1155.
53. Cavasotto, C. N.; Orry, A. J.; Murgolo, N. J.; Czarniecki, M. F.; Kocsi, S. A.; Hawes, B. E.; O'Neill, K. A.; Hine, H.; Burton, M. S.; Voigt, J. H.; Abagyan, R. A.; Bayne, M. L.; Monsma, F. J., Jr. *J. Med. Chem.* **2008**, *51*, 581.
54. Monti, M. C.; Casapullo, A.; Cavasotto, C. N.; Napolitano, A.; Riccio, R. *ChemBioChem* **2007**, *8*, 1585.
55. Rossi, M.; Rotblat, B.; Ansell, K.; Amelio, I.; Caraglia, M.; Misso, G.; Bernassola, F.; Cavasotto, C. N.; Knight, R. A.; Ciechanover, A.; Melino, G. *Cell Death Dis.* **2014**, *5*, e1203.
56. Li, W.; Cavasotto, C. N.; Cardozo, T.; Ha, S.; Dang, T.; Taneja, S. S.; Logan, S. K.; Garabedian, M. J. *Mol. Endocrinol.* **2005**, *19*, 2273.
57. Abagyan, R.; Argos, P. *J. Mol. Biol.* **1992**, *225*, 519.
58. Jorgensen, W. L.; Chandrasekhar, J.; Madura, J. D.; Impey, R. W.; Klein, M. L. *J. Chem. Phys.* **1983**, *79*, 926.
59. Hornak, V.; Abel, R.; Okur, A.; Strockbine, B.; Roitberg, A.; Simmerling, C. *Proteins* **2006**, *65*, 712.

60. Wang, J.; Wolf, R. M.; Caldwell, J. W.; Kollman, P. A.; Case, D. A. *J. Comput. Chem.* **2004**, *25*, 1157.
61. Jakalian, A.; Jack, D. B.; Bayly, C. I. *J. Comput. Chem.* **2002**, *23*, 1623.
62. Case, D. A.; Darden, T. A.; Cheatham, T. E. I.; Simmerling, C. L.; Wang, J.; Duke, R. E.; Luo, R.; Walker, R. C.; Zhang, W.; Merz, K. M.; Roberts, B.; Hayik, S.; Roitberg, A.; Seabra, G.; Swails, J.; Götz, A. W.; Kolossváry, I.; Wong, K. F.; Paesani, F.; Vanicek, J.; Wolf, R. M.; Liu, J.; Wu, X.; Brozell, S. R.; Steinbrecher, T.; Gohlke, H.; Cai, C.; Ye, X.; Wang, J.; Hsieh, M.-J.; Cui, G.; Roe, D. R.; Mathews, D. H.; Seetin, M. G.; Salomon-Ferrer, R.; Sagui, C.; Babin, V.; Luchko, T.; Gusarov, S.; Kovalenko, A.; Kollman, P. A.; University of California: San Francisco, 2012.
63. Phillips, J. C.; Braun, R.; Wang, W.; Gumbart, J.; Tajkhorshid, E.; Villa, E.; Chipot, C.; Skeel, R. D.; Kale, L.; Schulten, K. *J. Comput. Chem.* **2005**, *26*, 1781.
64. Ryckaert, J.-P.; Ciccotti, G.; Berendsen, H. J. C. *J. Comp. Phys.* **1977**, *23*, 327.
65. Srinivasan, J.; Cheatham, T. E.; Cieplak, P.; Kollman, P. A.; Case, D. A. *J. Amer. Chem. Soc.* **1998**, *120*, 9401.
66. Vorobjev, Y. N.; Hermans, J. *Biophys. Chem.* **1999**, *78*, 195.
67. Qiu, D.; Shenkin, P. S.; Hollinger, F. P.; Still, W. C. *J. Phys. Chem. A* **1997**, *101*, 3005.
68. Feig, M.; Brooks, C. L., 3rd. *Curr. Opin. Struct. Biol.* **2004**, *14*, 217.
69. Miller, B. R.; McGee, T. D.; Swails, J. M.; Homeyer, N.; Gohlke, H.; Roitberg, A. E. *J. Chem. Theory Comput.* **2012**, *8*, 3314.
70. Metz, A.; Pfleger, C.; Kopitz, H.; Pfeiffer-Marek, S.; Baringhaus, K. H.; Gohlke, H. *J. Chem. Inf. Model.* **2012**, *52*, 120.
71. Zhang, J. H.; Chung, T. D.; Oldenburg, K. R. *J. Biomol. Screen.* **1999**, *4*, 67.
72. Iversen, P. W.; Eastwood, B. J.; Sittampalam, G. S.; Cox, K. L. *J. Biomol. Screen.* **2006**, *11*, 247.

List of Captions

Figure 1. Structures of gefitinib (**1**), erlotinib (**2**), 4-unsubstituted pyrido[2,3-*d*]pyrimidin-7(8*H*)-ones (**3**), 4-amino-5,6-dihydropyrido[2,3-*d*]pyrimidin-7(8*H*)-ones (**4**), 4-aminopyrido[2,3-*d*]pyrimidin-7(8*H*)-ones (**5**), and 2,6-dichlorophenyl substituted pyridopyrimidines **6{1}** and **7**.

Figure 2. Favorable (magenta) and unfavorable (orange) poses of the ligand **6{1}** within the binding site (left panel). Interactions with the receptor for the favorable pose of ligand **6{1}** are shown on the right panel.

Figure 3. RMSD of “favorable” (blue) and “unfavorable” (red) poses of ligand **6{1}**, in complex with EGFR through 40 ns of the production phase (NPT ensemble, 1 atm, 300 K).

Figure 4. Binding pose of ligand **6{1}** (magenta color, receptor carbon atoms are in light grey color) overlapped with erlotinib (PDB: 1M17, left) and gefitinib (PDB: 2ITY, right). Residues Thr790, Gln791, and Met793 are shown in stick representation.

Figure 5. Time dependence of hydrogen bond (HB) distances between H atom and acceptor atom of hydrogen bonds present in favorable pose of ligand **6{1}** : N3...HN(Met793) (yellow), O(Met793)...HN (red), O(Gln791)...HN(C4) (blue), Oγ1(Thr790)...HN(C4) (green). In those bonds where the NH₂ group is involved, distance was measured only for one of the two H atoms.

Figure 6. Ligand **6{1}** within the binding side of EGFR showing the hindered rotation of aromatic ring A.

Scheme 1: Synthesis of pyrido[2,3-*d*]pyrimidines **6{x}**

Figure 7. Decomposition of the binding energies $\Delta G'$ (left) and the van der Waals contribution ΔE_{vdW} (right) on a pairwise energy decomposition scheme for **6{1}** (blue), **6{2}** (green), **6{4}** (yellow), and **6{10a}** (red).